Radiation Production Notes
Note 10

April 1971

Electron Beam Diagnostics Using X Rays

by
D. W. Forster
M. Goodman
G. Herbert
J. C. Martin
T. Storr
Atomic Weapons Research Establishment

SSWA/JCM/714/162

1 INTRODUCTION

The X-ray spatial distribution produced by an electron beam hitting a high Z target has been used as a diagnostic for many years. Quite early in the development of very short pulse X-ray systems we used it to provide indications of the spot diameter and, a little later, the mean angle of incidence of the electrons at the anode. Physics International in particular have used the whole X-ray field to check electron flux and mean angle as a function of radius across the cathode, using low Z material to map the front surface dose and high Z to map the intermediate field, during the Aurora programme. Cornell have employed both framing and streak camera techniques to give a time-resolved pattern of the electron flux at the anode. Sandia Laboratory, Albuquerque, have used polar diagram diagnostics on Hermes II and have also used the spectral content of the X-ray flux to obtain time-resolved data on the energy of the original electron beam in the diode.

While many of the remarks made below apply to the high voltage range, the aim of this note is to extend the simpler of these techniques to the low voltage range and to point out their advantages and some of their limitations. It is intended to be a user's note and will concentrate on the practical issues involved; consequently it is redolent with simplified treatments and adequate approximations which ease the reduction of the data. It is also parochial in that it lays out the parameters we use and how we obtain them on a routine basis. It is hoped that the justifications offered will explain our choice but, as with all simplistic parameters, many can, in principle, be used.

Section 2 deals with the beam parameters which can be measured and in this section some of the techniques possible will be outlined, although we have not yet found it necessary to use them all.

Section 3 covers the experimental data for the X-ray generation from an axial beam of electrons and the way this is treated to analyse experimental results.

Section 4 deals with some of the many practical aspects and attempts to assess the accuracy obtainable.

The last section deals with some experimental results obtained at AWRE as illustrations of some of the simpler applications.

This note is not intended to be the last word on the subject and, as such, the accuracies aimed at are of the order of 10 per cent rather than 1 per cent. However, in view of the fact that the mean angle of the electrons in a high flux beam can be obtained easily, such an accuracy is a very considerable improvement on previous techniques, while at the same time being quick and convenient.

2 OUTLINE OF DIAGNOSTIC TECHNIQUES TO BE CONSIDERED

The parameters which can be measured are the current density across a plane, the mean angle of arrival of the electrons as a function of the radius and also the energy of the electrons, all of the measurements being time dependent if required. While separate experiments may sometimes be required, several of the measurements can usually be done at the same time, at the cost of more recording channels. The great advantages of the techniques are that they can be employed at flux levels which will vaporise any material and also that the measurements are not restricted to the plane of the anode, but can be employed at the end of any transported beam.

The following list of experimental techniques covers and comments very briefly on some possible approaches.

2 a SPECIAL DISTRIBUTION

In general, a high Z target is used for these measurements, so that a flat polar diagram is obtained. For time integrated results a pin hole camera can be employed, using a series of films within it to cover a large range of intensities. Because radiographic film has a high contrast ($\gamma = 3$ typically) and variations of density of a percent or two can be detected, rather high accuracies can be obtained for the resulting time averaged electron flux. The resolution can frequently be 10^3 to 10^4 elements if sufficient intensity is available to use small pin holes, which can be conveniently made in heavy metal. A lower resolution technique is to cover the high Z converter with dosimeters, of which TLDs are a very compact, cheap and convenient example. If these are required to respond to only small areas of the beam, they can be set in a high Z egg box structure, but in general it is adequate just to strap them on the rear face of the converter. For time dependent measurements an image intensifier camera may be used, either in the framing mode or in a streak mode. A thin slab of plastic phosphor is mounted on the back of the converter and light from this recorded. Unfortunately, as the voltage on the diode changes, large variations of the light output result. For a constant diode impedance the light will go roughly as the fourth power of the voltage and hence the camera has to cover as large a range of light intensities as possible. This may mean a number of separate image converter cameras, or possibly a camera with a series of images side by side with different optical attenuators in each of them; this, however, reduces resolution rather seriously.

In obtaining the electron flux from the data, the assumption has to be made that the energy of the electrons across the plane is the same and sometimes, as in the case of a diode pinched beam, it is conceivable that this is not so to an adequate accuracy. However, a subsidiary experiment using techniques given below can show if this is the case and provide a measure of the departure from a uniform instantaneous electron energy.

When using any spatial resolution techniques at voltages of several million volts the angle of the electrons at the converter becomes of paramount importance, since, even with a high Z target, the cone of X rays is small and may largely miss the detector from some area of the anode. This polar diagram vignetting can be of considerable importance in interpreting current distributions from an X-ray pinhole radiograph. This effect can also be of importance where a pinhole camera is added to other measurements in a low voltage shot using a low Z target, where again the polar diagram can be quite peaky. The dosimeter plot across the rear face of the converter is much less susceptible to this difficulty and can be very useful where the electron mean angles become significant compared with the polar diagram width. The corresponding time dependent measurement can be made in these conditions by using phosphor blocks in egg boxes on the rear of the converter and connecting these to photo-diodes or photo multipliers by shielded light pipes, or maybe it would be better not to do the experiment at all under the circumstances.

Another potential difficulty may arise in a drifted beam, where an original monoenergetic beam develops a spread of energies. This can conceivably come about from two-stream instabilities, or because of electrons being slowed at the front and/or being overtaken by faster ones from later in the pulse. In these circumstances the higher energy electrons produce most of the X-ray emission and the results are then biased towards the distribution of these. A subsidiary experiment of the kind outlined below can warn when this is happening.

2 b POLAR DIAGRAM MEASUREMENT OF THE MEAN ELECTRON ANGLE $\bar{\theta}$

For low Z materials the polar diagram is comparatively sharp, even for low energy electrons. For instance, for carbon, for a 1 MeV electron beam the half width at half height of the polar diagram occurs at about 27° and even for 0.2 MeV the angle is only some 57°. Thus mean angles as small as 10° can be measured with reasonable accuracy.

The polar diagram is ideally measured in the far field of the X ray pattern at a distance remote from the source. A fairly useful terminology, taken from rather longer wave e.m. usage is: near field - adjacent to the X ray source and within a fraction of its diameter; intermediate field - that which is neither near or far; and far field - where the source dimensions are small compared with the distance. The near field measurements have been covered above; the far field can be analysed to give $\bar{\theta}$; the intermediate field contains information relating to both the spatial distribution and the angular distribution of the incident electron flux at the converter. Ideally, measurements should be made all over the field and then unfolded, but life is a bit too short and hence the selection of one or the other region to simplify the data reduction. For polar diagram experiments there is pressure, because of dose limitations, to work

as close to the edge of the intermediate field as possible and then a spot size correction is taken off, a matter dealt with reluctantly in section 3. However, where the radius of the source is less than 10 per cent of the distance to the dosimeter array, the correction is small and reasonably well known.

To obtain a time averaged mean angle of the electrons, an array of dosimeters is set up at a constant distance from the source in one plane or, with asymmetric sources, two orthogonal planes. By comparison with the polar diagram to be expected from axial electrons the mean angle can be determined, as is discussed in section 3. In principle, distributions of electrons more complicated than a simple mean can be derived from the polar diagram, but experimental uncertainties render this a difficult and unrewarding task, except in a few special cases.

One of these is in the case of a pinched beam, where it can be estimated what fraction of the X rays come from the pinched phase; then two mean angles may be derived with reasonable accuracy. However, time dependent measurements, with or without blanking off of sections of the converter, can lead to better estimates. As dosimeters we use lithium fluoride TLDs and find these cheap, convenient and reliable.

In some beam transport experiments, stray dose may come from the outer regions of the converter or return conductors. These X rays can be shielded out with lead absorbers, or the TLDs mounted in lead telescopes so that they only see the intended converter area. As is mentioned in section 4, we use lightly shielded TLDs to reduce the response to stray background scatter X rays, but, if necessary, background TLDs shielded from the main source can be used to subtract out this component.

For time dependent polar diagrams a plastic phosphor photo-diode or photo-multiplier combination works well, the response of which can be separately calibrated or normalised with an adjacent integrating dosimeter.

The experimentally determined polar diagram is corrected for absorption in the converter, as is further explained in section 3, before being used to obtain a mean electron angle. However, a point worth dealing with at this stage is the definition of the mean angle and its relevance. As with all parameters which attempt to categorise a complex real situation with a single number, cases can easily be constructed where it is meaningless or misleading. However, as with the rise time of a voltage pulse, it is extremely useful to have such a parameter, accepting that it is only a rough approximation to real life. The real battle occurs when it comes to selecting the parameter. One possible choice is to assume that all the electrons are travelling at one angle and use this to fit the experimental pattern. This approach, in our experience, rapidly leads to highly non-observed polar diagrams for large electron angles. The parameter we use

is to assume that the electron flux uniformly fills a cone out to some angle θ_{max} . The relation between $\bar{\theta}$ and θ_{max} is not exactly constant but $\bar{\theta} = 0.65\ \theta_{max}$ is within a couple of per-cent as θ_{max} goes from 0° to 90°. Experimentally, this parameter appears to fit most of the data we have. In addition, considerations relating to electron trajectories in diodes and beams tend to suggest a fairly well smeared out distribution of electron angles. A sharp cut off at θ_{max} is practically very unlikely, but an angle above which there are few electrons is quite reasonable, if only in some cases because 90° is a limit for a progressively minded beam. Incidentally it is worth pointing out that a mean angle of 57° corresponds to a cone filled out to 90°.

2 c ANODE CATHODE VOLTAGE

The X ray dose rate for paraxial electrons is given by a relation of the form $dR/dt = k\ i\ V^n$ where $n = 2.8$ over a wide range for all materials and k is a function of the material. The values for these are discussed in section 3. If i is measured as well as dR/dt , then V is obtainable. Indeed, because of the high power of V a 10 per cent accuracy in the dose gives V to about 4 per cent. For a beam of electrons which is not axial, a polar diagram measurement made at the same time allows a correction to be made to allow for this. This correction can be made in two ways. If the polar diagram leads to a unique value for $\bar{\theta}$ this can be used to correct the dose on axis to what it would have been if the electrons were paraxial. A theoretically sounder method is to integrate the total flux of X rays and then use this integral radiated X-ray energy to give the incident energy of the electrons. Unfortunately, a lot of the X ray energy is radiated at large angles, even when the polar diagram is fairly peaky, and this may mean making measurements on the beam side of the converter. Absorption corrections in the target can also become important and tiresome; so, while this is sounder in theory, in practice the simpler procedure can be practically as accurate and a lot less trouble.

Experimentally a mean anode cathode voltage can be obtained with a dosimeter array and an approximate knowledge of the diode impedance, or a measurement of the mean current. However, if the converter is made part of a Faraday cup current monitor and if the dose on axis is measured by means of a phosphor photo-diode combination, the voltage can be obtained as a function of time. An example of this is given in section 5, where the mean angle of the electrons was small and hence the time-dependency of it was unimportant. Where this is not the case, a time-dependent polar diagram measurement is also required, so a Faraday cup converter and a phosphor photo-diode array is then required.

Where the electron flux is not too intense, the carbon block which doubles as an electron stopper in the Faraday cup and an X ray converter can also function as a calorimeter.

The main difficulty with this measurement is the accuracy of the constant k and the determination of the absolute dose rate. However, accuracies of $\pm$ 20 per cent in k are probably on with existing data, corresponding to an accuracy of $\pm$ 7 per cent in V. However, if the technique becomes popular, this constant can obviously be measured with entirely acceptable accuracy, although care will have to be taken in defining the experiments to make the new measurements of immediate practical use.

2 d ALL SINGING, ALL DANCING MEASUREMENT

Set ups can be devised which measure just about everything that is worth measuring, at least as far as the diode is concerned. Such a set up would involve an anode divided into, say, 3 equal sectors by sheets of lead orthogonal to the converter and containing the axis of symmetry of the beam. Within each 120° sector, lead shields are placed over the converter, letting X radiation out from 3 annular zones, one in each sector. The converter is in the form of a 3 sector carbon Faraday cup and measures the current to each carbon zone from which the radiation is being allowed to reach its corresponding photo-diode dosimeter array. There are 3 of these, each of which measures half of the polar diagram from one sector zone. From such a set up the values of $\bar{\theta}$ and the electron energy may be obtained as a function of time and of radius, providing the beam is axially symmetric. Yet more complicated set ups can be visualized, but it is doubtful whether there is any practical application for them - a comment which may well apply to the last proposal.

The approaches outlined above are in fact all fairly easy to set up and, as has been mentioned earlier, yield data for beams of extremely high fluence. While attention has been drawn to a lot of possible snags and difficulties, in practice they are easy to use and reasonably unambiguous in interpretation. Used in conjunction with standard tube voltage measuring techniques, they give real confidence in the internal consistency of diode characteristics, as well as providing values of $\bar{\theta}$ simply, for diodes and beams under most conceivable experimental conditions such as magnetically confined ones.

3 EXPERIMENTAL DETERMINATIONS OF POLAR DIAGRAM AND DOSE ON AXIS

As input for the analysis of X ray diagnostics, the polar diagram for axial monoenergetic electrons for various target materials is needed, as is the dose on axis. The two papers containing most of the available data are: Buechner et al., "Thick Target X-Ray Production in the Range from 1250 to 2350 Kilovolts" - Phys. Rev. 74, No. 10, Nov. 15, 1948; and Rester and Dance, "Thick Target Bremsstrahlung produced by Electron Bombardment of Targets of Be, Sn and Au in the Energy Range 0.2 to 2.8 MeV" - Jnl. App. Phys. Vol. 41, No. 6, May 1970. Comparison of these shows that the polar diagram data is in essential agreement and

fits rather well the Universal Polar Diagram of Limited Applicability, even down to 0.2 MeV. However, the data for dose on axis is in a considerably less satisfactory state and while the dependency on Z is very similar in each paper, the absolute agreement is poor.

A few general points will be made before proceeding to the comparison of the results. Buechner and his colleagues rotated the target, and the detector, which was mounted at right angles to it. Thus the self-absorption of the target changed only a little and they quote results where this has been removed. Rester and his partner fixed the target at right angles to the beam and moved the detector around it. Their results are quoted for external radiation uncorrected for target absorption. One main aim of their paper was to measure the spectra of the X rays and these are compared with ETRAN 15, consequently they used a NaI anticoincidence counter, from which the integrated energy flux was subsequently calculated.

Dealing first with the polar diagram results, a point which immediately arises is whether the data required should take a form corrected for target self-absorption, or as externally measured. If the data is quoted for external radiation this will clearly depend on the target thickness used and also the solid angle subtended by the detector. Moreover, as the target is viewed from the front face or the back face there will be a big difference in absorption, since in the latter case the X rays have to travel through much less absorbing material. Thus no form of universal curve will result as the transition from front face measurement to back face will occur at different points up the curve for different energies and Zs. Consequently we have elected to follow Buechner and remove the target absorption for the polar diagram results, otherwise ideally an ETRAN run would be needed to compare polar diagram results for each case. The consequence of this decision is that for any polar diagram experimentally obtained the target absorption must be allowed for, but for low Z materials this is a small correction, even out to 75°. This is, of course, the case of most interest for determining $\bar{\theta}$. However, even for high Z materials the correction is not large; for instance, even for 0.2 MeV at an angle of 60° it amounts to about 1.25 with an electron range thick target. Thus the correction for target and other backing material absorption is left to the experimenter, although guidance is given on it later.

The data of Rester on polar diagrams is given on p.2690, but before the polar diagram can be extracted one must take into account the fact that the backwards X ray flux comes from about one-sixth of the way through the target, while the forward flux passes through more like five-sixths on average. This effect is only of importance for the higher Z targets, namely tin and gold. Using the experimentally determined spectra given earlier in the paper, the absorption was removed at the small and large angles. A smoothed curve was used to join these points. The

same was done for the low Z targets and from these the polar diagrams in the absence of target absorption were obtained. These were then compared with the "universal" curve originally obtained from Buechner (SSWA/JCM/711/149). Again, the Z dependency factor of $(Z/74)^{0.30}$ was used and the data were plotted against $U\theta$ where $U \equiv V + 1/2$ and V is the electron energy in MeV. Figure 1 reproduces the "universal" polar diagram and figures 2, 3 and 4 give the Rester results obtained, as outlined above. Also shown in figures 2, 3 and 4 is the universal curve for an electron range thick target.

Even for 0.2 MeV the agreement is quite reasonable. There is a suggestion that for Be the curve is fatter than for the other materials, but the original points were taken from a very small scale graph and thus could be reading errors. However, at large values of $U\theta$ the low Z materials consistently lie beneath the universal curve. This had been noted for the Buechner data, but the scatter there was sufficient not to make the effect certain. The values for Au for 1 MeV lie above the curve significantly, but there the absorption correction may not have been quite correctly applied. Considering the original curve was partly based on data (high Z only) up to 27 MeV, the universal curve does a good job over a rather large energy range for this class of material. Within the originally stated accuracy of $\pm$ 10 per cent the curve fits the new data; however, for the case of particular interest, that is carbon, the polar diagram ratios below about 0.25 should be shifted to the left a bit. Figure 5 gives our best estimate of the polar diagram curve for an electron range thick target of this material. Also included are the results of an ETRAN calculation, kindly supplied by Dr Peter Fieldhouse and Mr David Large of CNR, for 2 MeV. The calculations were done with and without absorption and these gave essentially the same results as expected.

We now turn to the question of the dose on axis from axial electrons. The Buechner data had been analysed to give a $(Z/74)^{0.50}$ dependency. Figure 6 gives the smoothed on axis data. Also included is the data of Rester as given and also corrected for target absorption. (Note that the 0.2 MeV data has been multiplied by 10). Dodging the question of absolute yield for the moment, the two sets of data have been normalised at 2 MeV. The data is in very reasonable agreement as regards Z dependency and also shows that the slope is reasonably constant for $1.25<V<2.35$, but for low values of V the slope rises. The slope of the lines is slightly higher than 0.50 because these curves are for zero absorption. When the intrinsic absorption of the optimum high Z target is included, as is shown later, the slope is a bit lower and this is the one quoted on Figure 1.

In order to compare the absolute output on axis, the data in both papers have been converted to Roentgen at 1 metre per coulomb. The conversion for Buechner is simple, but the data from Rester is a bit more complicated. This has been analysed firstly

for a cut off of 0.05 MeV. This value is taken because below this value most detectors become rather sensitive to low energy X rays, and because any scattered field is usually in this range, it is desirable to cut off the low energy response. This point is dealt with further in section 4. The data is then converted, using as a factor $1\ R = 2 \times 10^9\ MeV/cm^2$. This is a reasonable average for X rays from 0.06 to 2 MeV. In addition, of course, the correction for target absorption is employed to make the data comparable. When this is done, the dose levels are very different, Rester's data being 1.62 times as large as Buechner's on average. This is troubling but, being unable to suggest that either set of data is greatly better than the other, some sort of average has to be taken. It is true that Rester's experiments are much more recent but the dose is more derived than that of Buechner's. When two sets of data are this far apart, it is a good question as to what average should be employed: we have elected to use a geometric mean, multiplying the results of Buechner by 1.27 and that of Rester by 0.79. Table I gives the data so treated for 0.2, 1 MeV and 2 MeV. The Buechner data has been extrapolated to give the data for 1 MeV for comparison with Rester's. In addition, Rester's data has been interpolated to given values for the Zs used by Buechner.

TABLE I

DOSE ON AXIS FOR AXIAL ELECTRONS
(IN ROENTGEN AT 1 METRE PER COULOMB)

E MeV	Z	4	13	26	47	74
0.2	Rester	2.5	9.5	18.5	27	44
1.0	Buechner	276	575	1010	1430	1810
	Rester	314	630	1020	1340	1730
	Average	295	600	1015	1380	1770
2.0	Buechner	2240	4250	7050	8000	10400
	Rester	2520	4340	6600	8000	10200
	Average	2380	4300	6800	8000	10300

To obtain the dose on axis from real targets it is necessary to include the absorption. As was mentioned in the original polar diagram note, it is possible to have an "optimum" target for high Z materials where a thin layer of converter is backed by a low Z material. For high voltage electrons (V > 10 MeV) this two layer optimum thickness is one-third of the radiation length and for tungsten this thickness is 2 grams/cm^2. For low Z materials this is impracticable and unnecessary because self-

absorption in the converter is very much lower, so the target is made an electron range thick. It may be worth while saying a few words about electron ranges at this point. The universally quoted range tables are for aluminium, with the statement that the range is largely independent of Z. The range most often quoted is the practical range which for 2 MeV electrons in aluminium is 1.0 gm/cm^2. However a significant number of electrons get beyond the practical range and the extrapolated range, which is what is needed essentially to stop the electrons, is about 1.2 gm/cm^2. However, for high Z materials the extrapolated range is more like 1.5 gm/cm^2 at 2 MeV, thus a fair degree of confusion can arise as to what is an electron range thick target. These elaborations are not relevant to the polar diagram data because the width is only a weak function of the thickness of the target. However, for the dose on axis the question is of significant importance. However, this sensitivity only applies for high Z targets and is avoided if the data is quoted for the optimum two layer target. This is also of considerable practical interest since this is the target which gives the largest dose on axis, which is normally the name of the game when high Z converts are being employed.

Figure 7 shows some data kindly supplied again by Dr Peter Fieldhouse and Mr David Large from an ETRAN run for 2 MeV electrons. It gives the generation of dose as the electrons move through the target (no absorption curve) and also the transmitted X ray flux (with absorption curve). These show the low self-absorption of a carbon target and also that the optimum thickness for a high Z target is again about one-third of the extrapolated electron range. Calculations suggest that the optimum target for a high Z material continues to be about one-third range thick and that the output level is about that appertaining to the 2 MeV case, or a little lower. This applies where a cut off of 0.05 MeV is again used.

Using the data in Table I, the output for a full range carbon target and for an optimum tungsten target can now be obtained and these values are given in Table II.

TABLE II

DOSE ON AXIS FOR PARAXIAL ELECTRONS
(IN ROENTGEN AT 1 METRE PER COULOMB)

Z	E = 0.2 MeV	1.0	2.0
W optimum target	28	1.17×10^3	6.9×10^4
C full range target	3.7	3.5×10^2	2.6×10^3

These results are shown in Figure 8 where the dose per coulomb is plotted against V . For the high Z target, Tom Martin of

Sandia has shown, in SC-DR-69-240, that up to about 30 MV the dose goes at $V^{2.8}$ and the intercept at 1 MeV agrees with that given by Tom Martin for the optimum target. However, for voltages rather less than 1 MeV the dose from a high Z target goes as a lower power. The carbon data, over the range it is available, goes as $V^{2.8}$. Because of the change of power of the on axis dose for tungsten for voltages below 1 Mv, the relation for the Z dependency of the dose given before as $(Z/74)^{0.50}$ does not apply. However, above 1 MV the relation is approximately true. If the carbon curve continues to rise as the 2.8 power of the voltage, the Z dependency will continue to hold. A rather rocky justification for the averaging used is the fact that the high voltage data for high Z optimum targets joins smoothly with the low voltage data. However, despite this consideration it must be reckoned that the dose relationship shown in Fig. 8 is uncertain in absolute terms. An error of $\pm$ 15 per cent in the dose axis is probable and it could well be higher.

Thie completes the analysis of the input data needed to use the X ray diagnostic techniques. In general, the agreement is reasonable but the dose on axis badly needs supporting by better data.

One of the incidental points which has not been covered so far is the dose produced by beams which are non-orthogonal, in particular for carbon. For high Z targets a large fraction of the electrons can be back scattered at small angles of incidence. However, in order to scatter out of the target, the electrons have to undergo a number of small angle scatterings, or a single large angle scatter. In both cases their energy is significantly reduced and because of the powerful law of X-ray production efficiency, an electron leaving with even half its energy will have generated most of the X rays that it can. Thus the generation of X rays should not be seriously affected when the beam is incident on the target at considerable angles. The argument is very much stronger for low Z targets when a smaller fraction is back scattered. These contentions are supported by Buechner's data, where the target was rotated so that the electrons were sometimes incident on it at small angles to its surface. The polar diagrams given by Buechner are smooth through this region, even for high Z materials. Thus the fact that electrons are non-orthogonal should not change the efficiency of generation of X rays significantly.

Figure 9 gives the normalised spectrum of X rays for 0.2 MeV to 3 MeV for carbon at 0°. However, the spectrum holds pretty well out to 45° or more. This curve is of use for absorption calculations and is taken from Rester's paper.

The above section deals with the required input data: what follows is an outline of how we use this data to derive the required beam parameters, in particular $\bar{\theta}$. A few words ahead of section 4 may serve to justify some of the rather crude approximations

we employ. Basically the data points have an error of the order of ± 4 per cent when sensible numbers of TLDs are employed. To achieve even this accuracy may mean the deployment of 20 to 30 TLDs. Some error in the input polar diagram must also be assumed to be present and these basic limitations imply that over-refinement in the treatment of the data is unnecessary. In addition, the basic assumptions in defining the parameter selected to categorise the mean angle also obviously have limitations, since while Nature is kind and tends to provide an approximation to a fully filled cone, she cannot be relied upon for slavish fulfilment of this requirement.

With these rather transparent justifications for our laziness, we now reveal all.

SELF ABSORPTION CORRECTION

Firstly the correction to the polar diagram for converter self absorption will be discussed. What is required here is the difference in X ray path length between the on axis X rays and those at any other angle. The X rays are assumed to be produced in about 0.2 of the electron range through the target on average. The extra path length is then easily calculated for the target and any other backing material. For carbon and other low Z elements, the absorption is rather small and while it is a little difficult to decide what cross-section should be used, it is fortunate that it does not matter much. The complication is that for low Z materials the interaction is mainly Compton scattering and hence a build up field of softer secondary X rays is developed. For infinite media the build up factors are well known but for thin slabs these calculations are not applicable. A second problem is that the build up field is largely isotropic and thus tends to reduce the peakiness of the polar diagram by X rays scattered into the large angle TLDs. This effect is mitigated by the use of copper shields around the TLDs, to some extent, but is still present. Figure 10 shows the absorption factor for carbon (and other light elements) as a function of thickness and original electron energy and was derived from Figure 9 and the published X ray total cross-sections. Again, a cut off at 0.05 MeV has been used. The absorption factor used here, and later, is the reciprocal of the actual absorption and is the factor by which a data point should be multiplied to remove the absorption effect approximately. As can be seen, for 1 MeV and a target of the order of the electron range thick, the correction factor is 1.05. For a point at 60° this is also the factor which would account for the extra absorption, if the full cross-section were to be employed. However, as has been stated, a lower factor than this applies and effectively we use two-thirds of the total cross-section. This fudge factor was derived from some very crude calculations of the build up factor and its effect on the polar diagram shape. Thus, in this case the 60° data would be raised by only 1.03. For high Z targets the situation is easier, since most of the absorption is photo-electric

and here the full cross-section is used to obtain the attenuation factor. In the experimental data given in section 5 the error bars for the points at 45° and 60° have been increased to allow for the plausible range of the attenuation correction factor.

For the dose on axis the curves give the value for an electron thick target for additional absorbers and the situation is different because the scattered X rays are essentially lost where a relatively peaky polar diagram occurs and, typically, a cross-section equal to the total cross-section is used in such cases. Again, for high Z additional absorbers the full absorption factor would be used.

DETERMINATION OF $\bar{\theta}$

Using the experimental data corrected to a zero absorption target, the normalised polar diagram is plotted against θ. On the same graph the axial electron polar diagram is plotted (using Figure 5 if the target is carbon). This raises the question as to what V_{eff} should be employed. It is not difficult to derive a series of polar diagrams for the real time varying electron energy, but if the anode cathode impedance is constant a value of V_{eff} equal to 0.84 V_{max} is a good approximation.

The question now arises as to what the polar diagram is for various values of $\bar{\theta}$ for the incoming electrons. A series of calculations for the fully filled cone and for other reasonable distributions has shown that the following approximation is an adequate one.

For the 0.75 level add 0.9 $\bar{\theta}$
For the 0.50 level add 1.0 $\bar{\theta}$
For the 0.25 level add 1.1 $\bar{\theta}$

Using this approximation, curves are easily constructed from the $\bar{\theta} = 0$ curve for various values of $\bar{\theta}$. Figure 14 gives an example of the results and shows that the experimental data fits a mean angle of a little over 10° rather well.

If the above scheme offends people's sensibilities, Tom Martin, in SC-RR-69-241, gives a computer code for predicting the X ray polar diagram. The polar diagram used in his report is slightly different from the one advocated in this note and in the examples calculated explicitly the spot size is also made a function of the voltage, but this is not inherent in the treatment. However, because of the factors mentioned earlier, it is believed that the approximation used in our approach is sufficiently good, especially for low values of $\bar{\theta}$.

SPOT SIZE CORRECTION

In general, the dosimeter array should be at a distance at least 10 times the spot radius and preferably more. Where this applies, the spot size contribution to the polar diagram flattening is quite small and roughly equals $\theta \sim 57\ r/d$ degrees, where r is the effective radius of the spot and d the distance to the dosimeter array. The effective radius is two-thirds the outer radius for a uniform spot and equal to the mean radius for an annular spot. Once again, providing the correction is small, it does not matter exactly how you get it. This spot size correction is then taken away from the observed $\bar{\theta}$ to give the mean angle for the electrons incident on the target.

DOSE ON AXIS MEASUREMENTS

Firstly any absorption over and above that in the optimum target (high Z) or electron range target (low Z) must be allowed for, as is indicated above. Then a correction has to be applied for the effect of the mean angle of incidence of the electrons. This correction involves the real angle and hence cannot be applied directly to the universal curve. This has first to be reinterpreted to give the polar diagram against laboratory angle for the material and electron energy used and then weighted by a sin θ factor and averaged. Figure 11 gives as an example the drop in on axis dose for a carbon target as a function of $\bar{\theta}$ and energy of the electrons. The observed dose is divided by the appropriate factor to yield what would have been dose on axis for axial electrons.

As was mentioned earlier, the other way to treat the problem is to integrate over all solid angles and obtain the total radiated flux, but for the reasons mentioned before we prefer the above treatment in cases where the polar diagram yields a reasonably unique value for $\bar{\theta}$.

For most of the cases we have been interested in this factor is small and even when it becomes large, uncertainties in it only enter the resulting derived electron beam energy as the one-third power, approximately. Thus it does not contribute significantly to the uncertainty of the final answer, certainly not when compared with the basic uncertainty in X ray generation efficiency covered in the first part of this section.

In concluding this section we would like to mention that the particular shape of the universal curve, coupled with the fact that basically an integration of it is being made to allow for the practically existing range of electron angles, means that for a widely varying smooth range of assumed electron distributions the curves look surprisingly similar. Also the half point of the polar diagram shifts by about the mean angle of the distribution. This fact enables the rather approximate treatments to give quite good answers; at the same time it implies that

details of the actual electron distribution cannot be extracted from an experimental polar diagram without great accuracy in the measured data and in the input data. This point is briefly returned to in section 5.

4 PRACTICAL ASPECTS AND ACCURACY

In this section the practical nitty gritty will be covered from an essentially parochial viewpoint. While the approaches we have employed are obviously not by any means the only ones that can be used, they are of course the only ones we can comment on with confidence. The aspects to be covered will be in roughly the order used in section 2, to which reference should be made for some of the practical aspects.

4 a SPATIAL FLUX DISTRIBUTION MEASUREMENTS

There are three main sources of error in taking pinhole radiographs, namely pinhole vignetting, polar diagram vignetting, and background on the film. The first one of these is fairly obvious but if care is not taken, a fall off of density towards the edge of the field of view can be interpreted as lack of flux rather than a too large ratio of length to diameter of the pinhole. It pays quite a lot to use the densest material in which to drill the pinhole and to have a series of inserts with different diameter holes in them. In the past we have also used a rectangular array of pinholes of different diameters and with different absorbers over repeats of the same hole. This is quite useful for covering a large range of intensities and also ensuring that the X rays doing the photographic darkening have approximately the expected spectrum. In general we use a fraction of a mm of copper filtering to make sure that X rays from the tail of the pulse or scattered X rays do not have much effect. However, to prevent flux penetration through the front of a large multiple pinhole camera can be quite difficult and we now mostly use a high resolution camera and a low resolution one side by side.

Polar diagram vignetting was dealt with in section 2 and again can lead, unless care is taken, to an under-estimation of the spot diameter.

Even when these two effects have been eliminated or allowed for, it is still easy to make a mistake as to the spot size. This is because of the very high contrast of X ray film. For instance, a beam which diode pinches driving the pulse will produce a very intense black image; but this is surrounded by a diffuse halo of X rays which can easily contain as much, if not more, integrated flux. We therefore use 3 films in each of the cameras of varying sensitivity to check this point. The poor resolution camera can also pick up low area density records from say the anode plane or the drift cones and enable crude estimates of the fraction of the electrons hitting these to be made. Allowance of

course has to be made for the increased efficiency of production of the guide cone, if this is made of copper, compared with the main beam hitting carbon, and for any other extra absorption in the path of the X rays. Mention should also be made of the use of a large aperture camera at right angles to the diode or beam axis for the same purpose of pinpointing stray stalk emission or beam losses.

The third factor is background. In general quite a modest amount of lead shielding around the sides of the camera will prevent background scattered X rays getting in, but a check of this can be made by placing small lead absorbers up against the front of the film pack and midway between the film pack and the pinhole. While relatively modest thicknesses of lead prevent fogging from the back or sides, much larger quantities are required on the face of the camera, especially when small pinholes are used. In general we avoid using extremely small pinholes for this reason, otherwise absorptions through the front of 10^3 to 10^4 may be necessary. Such absorption factors can be obtained but the spectrum hardens considerably and hence becomes more penetrating. This difficulty particularly applies to systems working at 2 or 3 MeV. When a medium size pinhole is used, allowance for the effect of the penumbra can quite easily be made when the spot has sharp edges.

An additional source of error in deriving the edge of a spot applies where a central emitter is used, such as a small ball or a razor blade. In addition to any polar diagram vignetting, there is a cosine effect of flux arriving obliquely at the target, which again is amplified by the high contrast of the film. However, despite all these effects, quite accurate measurements can be made visually and, with film response calibration, quantitatively.

With regard to dose scans across the face of the target with TLDs, these give quite good relative results even when only placed against the back face of the target. However, some degree of local shielding with copper is desirable and of course the target must be at least an extrapolated range thick, so that electrons cannot get directly to the dosimeter material.

One point that is worth making is that the integral of the flux across the face in the near field should of course equal the integral of the flux in the far field. Where this does not happen (which in our experience is surprisingly frequently) two obvious explanations may be worth looking at. The first is that a significant fraction of the beam is hitting regions outside the nominal target area, with a low flux density. This of course can miss the array on the rear of the target but affect the polar diagram TLD array. A second possibility is that the superlinearity correction for the TLD may not be accurate and since the dose levels may well be 10^2 to 10^3 different, this will affect the close in readings much more than those of the polar diagram array.

4 b POLAR DIAGRAM MEASUREMENTS

The first and most obvious point here is that all the readings are referred to the reading on axis. If this data point is measured incorrectly due to variability in the TLDs, the whole pattern is thrown out. Consequently the number of TLDs at zero degrees should be higher than at the other angles. We find that unless special care is taken, the standard deviation for a single TLD is in the region of ± 5 per cent, providing the dose is in the range 0.5 to 500 R. Below this range the background correction on our TLD reader becomes significant and above it the super-linearity correction comes in. This is not to say that readings cannot be made above this range, but if they can be avoided it helps to increase the accuracy a bit. We deploy a symmetrical TLD array and if 2 TLDs are used at each angle and 4 at the zero angle position, the mean error for each angle (averaging the two minor image readings) becomes about 2 1/2 per cent and the error in a point normalised against the on axis dose is ± 3 1/2 per cent. To obtain much better than this requires a large number of TLDs. However, this accuracy is of the order of that of the polar diagram curves themselves and hence a reasonable balance between errors has been struck.

The second point concerns the shielding of the TLDs. We use copper pipe of 1 mm wall thickness and 6 mm bore. This arrangement dates from our radiographic days when we investigated an "air wall" arrangement and found that for X rays from about 4 MV electrons the absorption in the copper was balanced by the extra dose arising from the extra knock-on electrons getting through the polythene powder container and coming from the copper. Figure 12 gives the attenuation correction factor for th s thickness copper tube and also for a tube of half the thickness. The latter might well be preferable if measurements were being made around or under 0.5 MeV electron energy. Again these numbers are calculated for a cut-off in the original spectrum of 0.05 MeV, in conformity with the dose calculations. We have not made comparisons between the copper clad TLDs and the bare ones, but we feel that the cleanliness of the polar diagrams we obtain (such as in Figure 14) is partly because of this light local shielding. The effect of the copper shielding is to help to wipe out secondary scatter from the dustbin, etc. and also it avoids the region where corrections for the absorption of the LiF itself compared with an air dosimeter become necessary. Because we use an intermediate Z material of small thickness, the absorption is well known, being mainly photo-electric in the region where it is removing the low energy tail of X rays. Another factor that helps is that any low energy X rays from large currents flowing late on in the diode at low voltages are wiped out. Polar diagrams from single razor blades have been taken with the standard holders wrapped in additional lead shielding and these gave essentially the same curve as in Figure 14; they also showed that the spectral hardness was approximately what would be expected from the diode volts.

Time resolved measurements made with photodiodes are easy and reproducible. We use a 2" diameter ITT photodiode, type W114 and a block of plastic phosphor NE102 of about 2" diameter and 3" long, white painted on the outside. This is shielded on the outside by lead and on its face by about 0.5 mm of copper. The photodiode-phosphor combination has very constant characteristics and directly drives the oscilloscope deflection plates, since it can produce up to 3 amps linearly with about 2000 volts on the diode. The saturation current of the diode is over 7 amps and the turn over fairly sharp. Such a combination could readily be absolutely calibrated but we mount TLD near the phosphor in order to measure the integrated dose, whenever this is necessary.

4 c BEAM ENERGY MEASUREMENTS

The electron energy measurements basically require the absolute measurement of dose at a metre as well as the determination of the current in the diode, or, if a beam is used, with a Faraday cup. Some time ago we went through a lengthy comparison with other people's dose measurements, including Physics International and Harry Diamond Laboratories, and eventually felt we were within 5 per cent of the true dose. However, something like a man-year of effort was needed to attain this state (which aged the gentleman concerned by at least twice this amount) and while we think we are still about as accurate as this, this is more an act of faith than a statement of scientific certainty. What we did find, and have found since, is that other laboratories (neither of those mentioned, we hasten to add) can be up to 70 per cent in error and hence the measurement of dose at a metre is not something that can be tossed off in an afternoon, but is a fairly difficult activity needing continuous effort after it has been first achieved. Once again it is desirable to lop off the very low energy end of the spectrum, but where you do the lopping will be important if the technique is to be pushed down under 0.5 MeV. Also for very low X ray energies the thickness of the phosphor will have to be reduced (or allowed for) as the phosphor then essentially absorbs all the X rays, in the very low energy region. This is incidentally yet another reason for having a cut-off at some level, so that the phosphor is approximating to an air-wall chamber.

Thus the rather unexpected result of investigating the determination of the absolute rate of production of X rays is that the time dependency of the X ray flux is rather easy; the uncertainty lies in measuring its absolute level.

5 EXPERIMENTAL RESULTS

A representative series of experimental results will be covered in this section, partly as illustrations of the way the various calculations are performed, and partly as examples of the sort of data and consistency we obtain.

In the rather daunting Figure 13 the results from three particular shots are shown as plots of the experimentally obtained polar diagrams after correction for target absorption. The experimental set up was essentially the same in all three shots, a single 3.9 cm long razor blade being the cathode. A carbon block formed the anode whose mass was 0.75 gram/cm^2 approximately. The peak volts were about 1 MV but the current differed significantly between the shots. The TLD array had to be installed within a cylinder behind the anode (the dustbin) and so only a limited radius could be employed and this was 13.5 cm. Paired TLDs were used at each point and the angles used were $\pm$ 0°, 15°, 30°, 45° and 60°. Two arrays at right angles to each other were also deployed, one along the blade and the other at right angles to it. As it turned out, this was unnecessary, because of a compensation which took place, so that there were no statistically significant differences between the two orthogonal polar diagrams obtained. The probable explanation for this was that while along the blade the spot size was significantly bigger, the mean electron angle was low, while at right angles to the blade the spot size was smaller but the mean angle up. As such, the data points plotted in Figure 13 are the average of all 4 similar angle positions.

Taking Firing 750 first, this is representative of a well-behaved constant impedance shot. The anode cathode distance was 1.5 cm and the blade stuck out from the flat cathode plate 0.8 cm. The anode spot was well defined and 5.6 cm by 2.4 cm and in the form of a rectangle with rounded ends. The mean angle was about 10° or a little larger, about equally due to spot size and angular divergenc e of the beam at the anode. This point is gone into more deeply with respect to Figures 14 and 16 below.

Firing 742 had an anode cathode spacing of 0.75 cm and as such, exceeded the critical current for pinching during the pulse. As can be seen, the mean angle is now a little bigger than 20°, say 22°. Because the spot size will be rather smaller during the latter part of the pulse, the time-averaged mean electron angle has increased from something over 6° to more like 18°. As an illustration of the relative insensitivity of the polar diagram plot to details of the assumed distribution, Figure 13 also shows one line calculated as follows. It is assumed that for half the pulse the mean angle (spot size plus electron mean angle) is 10° and for the other half a value of 35° is taken. As can be seen, this assumption fits the data as well if not slightly better. However, one could not distinguish between the two possibilities on the basis of the experimental points. On the basis of other reasoning, the second possibility is a bit more likely. The way to distinguish between the two possibilities is, of course, to make time resolved polar diagram measurements.

Firing 747 again had an anode cathode gap of 1.5 cm but in this case significant current flowed during the prepulse, the prepulse gap broke down and applied a 50 kV prepulse, which in its

turn largely collapsed before the main pulse arrived. The current was several times larger than in a normal firing and it is expected that plasma filled the anode cathode region early in the main pulse, if not before. A strong diode pinch resulted and this is rather dramatically confirmed by the polar diagram measurements, which show a mean angle of about 60°, corresponding to a fully filled cone of 90° angle.

These three shots show the full range of angles that we have observed, although we are fairly certain we can produce beams with a mean angle of a degree or so, but whether the polar diagram input data is accurate enough to show such an angle is rather debateable.

The next example is Firing 818 which again is a single full length razor blade with an anode cathode gap of 1.5 cm. The anode was again an 0.75 gram/cm^2 carbon block but backed this time with 0.6 cm of lucite (Perspex for our English readers). The polar diagram obtained is shown in Figure 14. The calculated spot size angle is 6° and the estimated mean angle of the electrons at the anode is again 6°. The experimental points almost unbelievably fit a 12° total mean angle, which must be partly fortuitous. We should perhaps reassure the dubious reader that the new curve for carbon given in Figure 5 was derived from the Rester paper completely independently and the experimental points are entirely unadjusted apart from a very small target absorption correction for the 45° and 60° angles.

Figure 15 gives a welter of information. The voltage and current curves are derived from our normal monitors, the voltage curve having been corrected for the L di/dt as is usual. Also shown is the smoothed impedance curve with a rather satisfying constant impedance of about 50 ohms during the first pulse, which is highly characteristic of a single full length blade. There are two pulses because the 2 ohm generator is very lightly loaded. The climbing current during the second pulse is almost certainly associated with current emission from the cathode stalk. This is because some shots show that the razor blade on its own keeps a good impedance out to 300 ns; Figure 18 shows an example of such a shot. The carbon anode was also a calorimeter which recorded 1.3 kJ while the energy obtained by integrating the first pulse plus a small fraction of the second is 1.55 kJ. This difference is likely to be caused by calibration errors of the calorimeter but could be due to some 1 1/2 kA flowing other than from the razor blade cathode. Usually the system is operated at 100 kA or so; consequently we would not normally bother about such small background stray current flow.

Also given in Figure 15 is the photodiode pulse, normalised in amplitude to unity at peak and adjusted to fit the peak with regard to the zero time of the sweep. The current and voltage waveforms are accurately correlated in time but the photodiode record is not tied in with this system. From the polar diagram

TLDs, and others at 42 cm and 1 metre, the dose at a metre was measured to be 0.46 R with an estimated error of ± 10 per cent. The peak current was 19 kA and the effective pulse width (measured either from the photodiode record at 50 per cent height, or the voltage wave form at 84 per cent of peak) is 70 ns. Thus $Q_{eff} = 7 \times 10^{-8} \times 1.9 \times 10^{4} = 1.2 \times 10^{-3}$ coulomb.

From Figure 8

$$\text{Dose} = 3.7 \times 10^{2} V_{max}^{2.8} Q_{eff} = 0.46,$$

giving $V_{max} = 1.00$ MV.

Using the measured currents, the photodiode record is used to give the electron energy as a function of time and the peak voltage used is that derived above. The points so obtained are also shown in Figure 15. The error bars on these points are obtained as follows. Dose at 1 metre, ± 10 per cent input data, ± 15 per cent current, ± 7 per cent, giving an overall error in $V^{2.8}$ of ± 20 per cent and hence an error in the voltage of ± 7 per cent. The agreement obtained for the peak voltage is obviously a little fortuitously good, again, but the agreement as regards waveform shape is quite acceptable.

Summarising the results of this shot, we would conclude that our monitoring is in reasonably good shape and that indeed, as we had calculated, the razor blade cathode gives a cold beam with $\bar{\theta} \sim 6°$.

The next shot (F 824) to be described, while it has some minor lacunae in the interpretation, also has some interesting conclusions which, again, did not come as a surprise.

The set up was once more a single full length razor blade in the centre of the cathode backing plate, with an anode cathode spacing of 1.5 cm. Beyond a double 0.3 mil. mylar window was a drift region of 34 cm length. The outer return conductor for this was made up from bits to hand and is not what we would have designed. It took the form of a copper cone, entrance diameter 26 cm, coning down to 13 cm diameter over 15 cm length. This was followed by a parallel section 19 cm long made out of 5 mil. melinex covered internally by 1 mil. aluminium. At the exit window there was a carbon target-cum-calorimeter. Unfortunately this did not take the form of a Faraday cup current monitor because this was a shot sandwiched in another programme. One of the current monitors measured the anode-cathode current and another the current just behind the diode face. The drift region pressure was about 1 torr. The pinhole camera showed a clear X ray pattern on the target and no detectable X ray emission elsewhere. The X ray spot was slightly distorted from the original rectangle, with rounded ends, but was largely rectangular with dimensions 5.2 x 2.6 cm approximately and with the long

axis in the original razor blade direction, as would be expected. The polar diagram plot for this shot is shown in Figure 16. As the TLD array was now outside the dustbin, the radius could be increased to 20 cm, reducing the spot size angle to 4°. If the input data of section 3 is to be believed to the required accuracy, the mean electron angle after drifting remains at 6° or a fraction less. However, it can certainly be stated that it has not increased after drifting 34 cm. This is in line with previous measurements made on MOGUL and collectively remembered, that drifting did not significantly increase the mean angle of the beam. In both cases the ν/γ was about 0.4, although for MOGUL the mean voltage was like 4 MV and the present result is much more accurate. Thus we detect no transfer of energy to the perpendicular direction. The other possibility for two stream instability is that the beam energy is modulated in the direction of its propagation: this was investigated in the second part of the measurements, although here the proof that it did not happen significantly is not quite so direct.

Figure 17 gives the anode cathode voltage, current, and impedance, as measured by our standard monitors. Because the pressure in the tube was rather high and also because the false work is more than a little battered, the tube flashed around 70 ns. This is readily apparent from the current monitor beyond the tube vacuum interface. One of the effects that has been observed as a consequence of this is that more current apparently quickly flows in the anode cathode monitor loop. Whether this is genuine very fast plasma jetted from the tube interface, or the effects of a bar of much greater current (~1/2 megamp) advancing towards the anode cathode monitor, is not clear; it is perhaps connected with both effects. Anyway, it is considered that the fall in impedance after 70 ns is caused by the tube flash over and is not connected with the current flowing from the razor blade, which invariably has a constant impedance during this phase. Thus it is assumed that the cathode impedance stays constant at the flat level it had reached before 70 ns, as shown by the lightly dotted line. This is confirmed by the calorimeter reading, which was 900 joules. Multiplying by the factor previously found, this corresponds to about 1.1 kilojoules, while the expected beam energy was calculated to be about 1.15 kilojoules, using the reduced pulse length shown by the photodiode record. The excess current from the interface flashover, if it really is a current, would not enter the drift region - a fact confirmed by the lack of any extra X rays on the radiograph.

The dose at one metre was measured to be 0.28 R as an average of a number of determinations at different distances. Using the current deduced from a constant anode-cathode impedance of 58 ohms and this dose, the electron beam energy was calculated as before and is also shown on Figure 17. As before, the zero time of the photodiode record has been slightly shifted and the amplitude has not been normalised, but is obtained from the radiation

measurements. It should be noted here that if the full anode cathode current waveform had been used, the points beyond 70 ns would fall more sharply because of the increased current readings.

A point should also be made about the $L\,di/dt$ correction applied to the observed voltage waveform for times after 70 ns. As the monitor is mounted in the tube face, its record is held up by the large current starting to flow across the interface. The flashover was approximately opposite to the voltage monitor and hence there is a considerable inductance between the two. This makes determination of the $L\,di/dt$ correction uncertain after the insulator breaks down, so that the anode cathode voltage beyond this time is somewhat uncertain: the curve given is our best estimate. It might be supposed that the tube flashover was an unmitigated disaster, but in fact it was not. Two previous attempts to make the same measurement had failed, partly because extra emission had started from the cathode stalk during the second pulse, and on each occasion some of this had got into the drift region and messed up the polar diagram. So while it has rendered the interpretation a little less direct, it enabled a rather clear polar diagram to be obtained, and also where assumptions have to be made they do not disturb the major conclusion about a longitudinal variation in energy due to two-stream instability.

As is shown in Figure 17, the voltage waveform, deduced from the absolute photodiode record, lies, if anything, below the voltage monitor waveform. If the larger current values had been used, it would be even lower for times after 70 ns. Thus there is almost certainly no excess of dose on this shot. If a rather naive picture is taken that the beam splits into two equal populations, one with $V + \delta V$ and the other with $V - \delta V$, then the dose increase to be expected is $V(1 + 2.5(\delta V/V)^2)$. If any dose increase is taken as less than 10 per cent, and in fact the observed dose is some 15 per cent less than would be expected, then $\delta V/V$ is less than 0.2. The only way any significant spread of energy in the transported beam could be allowed is to reduce the mean energy of the beam as well. However, this is unlikely because of the calorimeter reading. Thus while we would be reluctant to claim that this firing disposes of any significant two-stream instability effects, it certainly does not support such effects and does suggest a technique of proving whether or not they occur. In such an experiment, the carbon block would be a Faraday cup and so measure the relevant current directly and accurately.

The last experimental example is not a very good one but it contains a couple of features of interest. On a number of shots we have had two bumps on the photodiode record, the second about 20 per cent of the first. Firing 819 was such a shot, although from several other aspects it was a rather unsatisfactory one on which to do an X ray voltage measurement. The set up in this

experiment was 6 half razor blades set out on the curve of the cathode plate. Beyond two 0.3 mil. aluminised mylar windows was a drift region with a series of 6 different guiding wire arrays. The pressure in the drift region was 0.17 torr and at the far end was a carbon target. Around the edge of this was copper foil and the copper wire supports. The average diameter of the array of beamlets was 20 cm but the pattern of each beamlet was, to say the least of it, complicated. Part of the beamlets hit the copper surround as well as the guiding wire supports. The energy transfer was good and, as before, anode cathode voltage and current measurements were made in the normal manner.

Figure 18 shows the peak voltage and also the derived smoothed diode impedance. Also shown in the electron energy measurement deduced from the two humped photodiode record. In this case both time and amplitude have been normalised at the peak. This was because of the big spot size and uncertainty as to what fraction of the beam hit copper rather than carbon. The normalised voltage derived from the photodiode record is not in good agreement in this case, but does follow in general the ordinary voltage waveform. The early high reading at 20 ns is probably because more of the beams were hitting the copper surround at the beginning of the pulse and the same explanation may well apply around 150 ns. The fact that the second derived voltage pulse is lower than it should be may well be because of small extra currents from the cathode stalk. Not altogether a convincing example but one which does display almost certainly a genuine double photodiode pulse.

The second point of interest in this firing is the way the impedance changes with time. The starting plateau, at about 16 ohms, is just about what we would expect. Normally a half razor blade has an impedance of 100 ohms at 1.5 cm and there were 6 of them and although these were at 1.8 cm from the anode foil they were in a diverging field. Thus the impedance per blade of 95 ohms, approximately, would be reasonable. The impedance climbs between the pulses and although the peak value of 30 ohms is rather dependent on the exact phasing of the V and i records, it is in the expected street. When the impedance falls again during the second pulse it is about 8 ohms. As the plasma blobs expand the specing decreases, and a small but significant droop would be expected in the impedance during the first pulse. However, we generally see a very flat impedance in this phase, or frequently a slightly rising one. This could be if the front of the plasma were developing a resistance in the region where the electrons were running away. However, when the current is drastically reduced between the pulses, this resistance may disappear. Anyway, taking the impedance change from 40 ns to about 220 ns, this implies a change of spacing of about 9 mm and hence a velocity of the order of 5 cm per microsecond for the plasma front, under these conditions of current density. This deduction is distinctly speculative but not out of line with expectations.

6 CONCLUSIONS

The various simple techniques outlined have a range of application for low voltage electron beam diagnostics. In particular they enable the mean electron angle and the electron energy to be determined as a function of time, almost regardless of the flux level. Certainly they can be used at much higher intensities than are necessary to vaporise any material. They are relatively simple to use and yield unambiguous results. Their range of applicability is from 0.5 MeV upwards and in some instances it may be possible to push the lower limit down to 0.2 MeV. They are a very useful adjunct to the normal monitoring techniques in diode and beam work but they should be used in conjunction with these, not as any sort of replacement. The results using them that we have obtained in the past agree with various other measurements and calculations and hence give considerable confidence that these are correct.

Various pitfalls await the unwary experimenter, but it is hoped that by now we have uncovered the more obvious ones. There is no guarantee that this technique washes whiter than all others, but with luck it will remove some of the stains from the experimental log book.

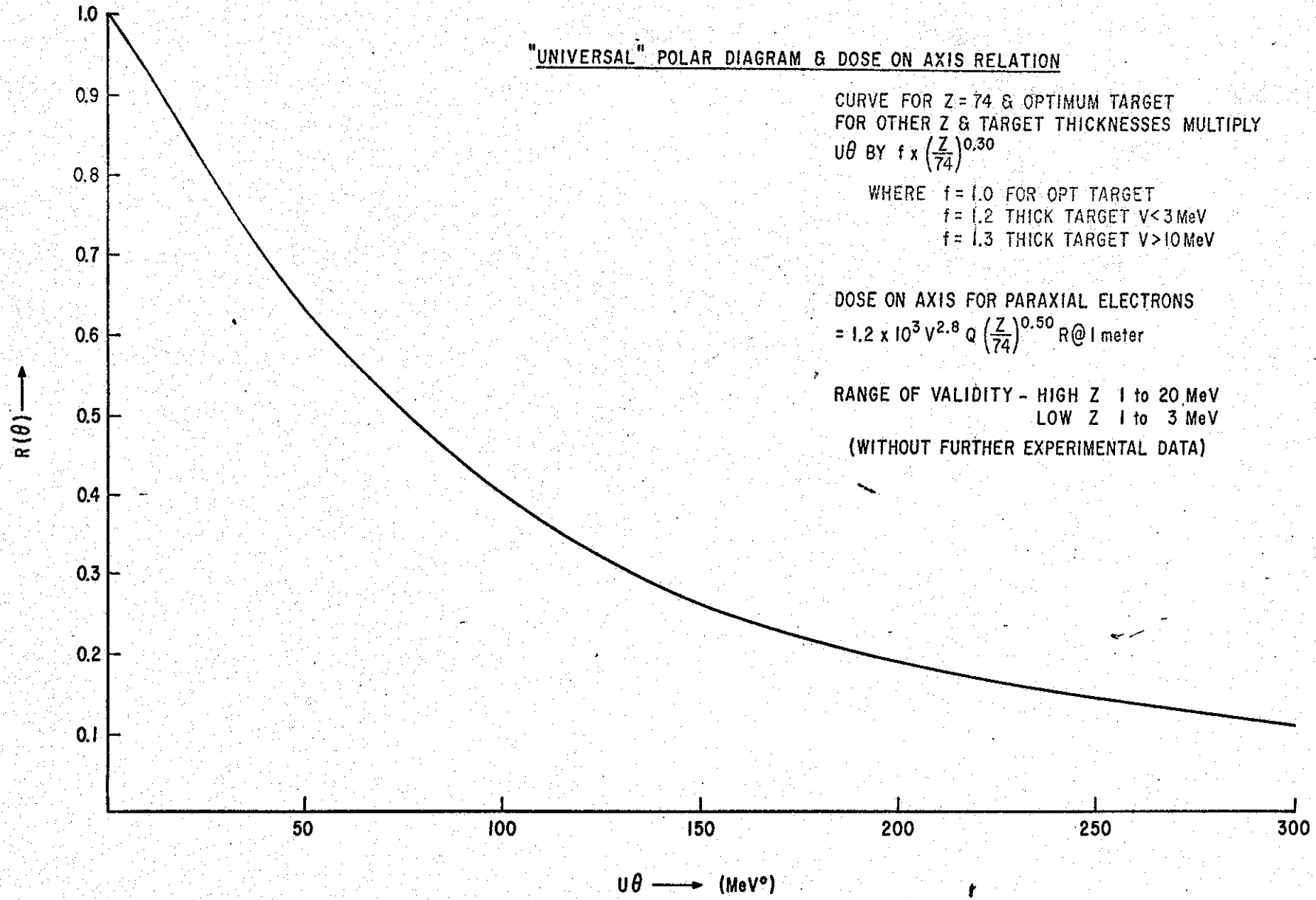
"UNIVERSAL" POLAR DIAGRAM & DOSE ON AXIS RELATION
CURVE FOR Z = 74 & OPTIMUM TARGET
FOR OTHER Z & TARGET THICKNESSES MULTIPLY
Uθ BY f x (Z/74)^0.30
WHERE f = 1.0 FOR OPT TARGET
f = 1.2 THICK TARGET V<3 MeV
f = 1.3 THICK TARGET V>10 MeV
DOSE ON AXIS FOR PARAXIAL ELECTRONS
= 1.2 x 10^3 V^2.8 Q (Z/74)^0.50 R@1 meter
RANGE OF VALIDITY - HIGH Z 1 to 20 MeV
LOW Z 1 to 3 MeV
(WITHOUT FURTHER EXPERIMENTAL DATA)
R(θ) ⟶
1.0
0.9
0.8
0.7
0.6
0.5
0.4
0.3
0.2
0.1
50
100
150
200
250
300
Uθ ⟶ (MeV°)

FIGURE 1

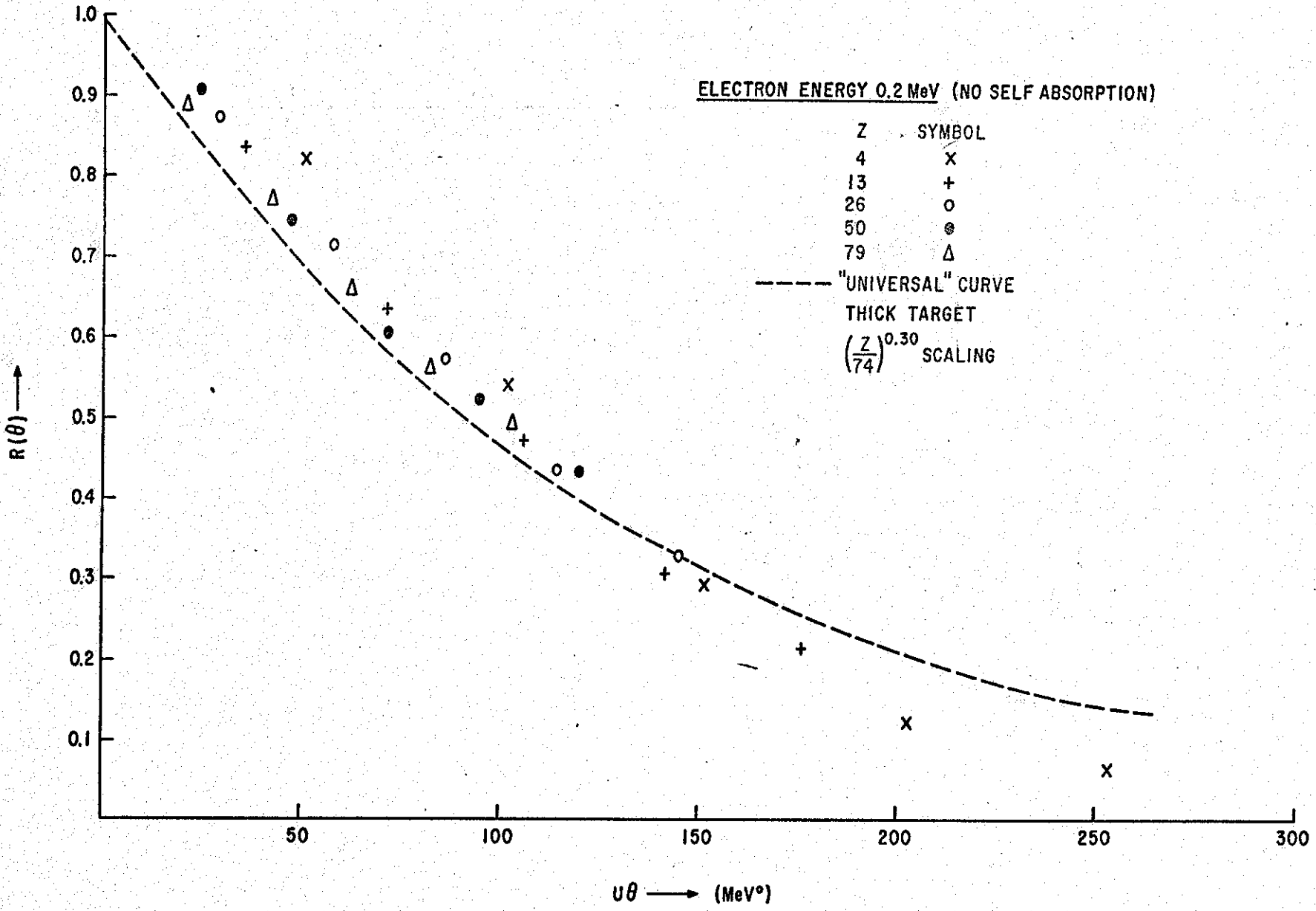
ELECTRON ENERGY 0.2 MeV (NO SELF ABSORPTION)
Z SYMBOL
4 X
13 +
26 o
50 ●
79 Δ
"UNIVERSAL" CURVE
THICK TARGET
$\left(\frac{Z}{74}\right)^{0.30}$ SCALING
R(θ) ⟶
1.0
0.9
0.8
0.7
0.6
0.5
0.4
0.3
0.2
0.1
50
100
150
200
250
300
Uθ ⟶ (MeV°)

FIGURE 2

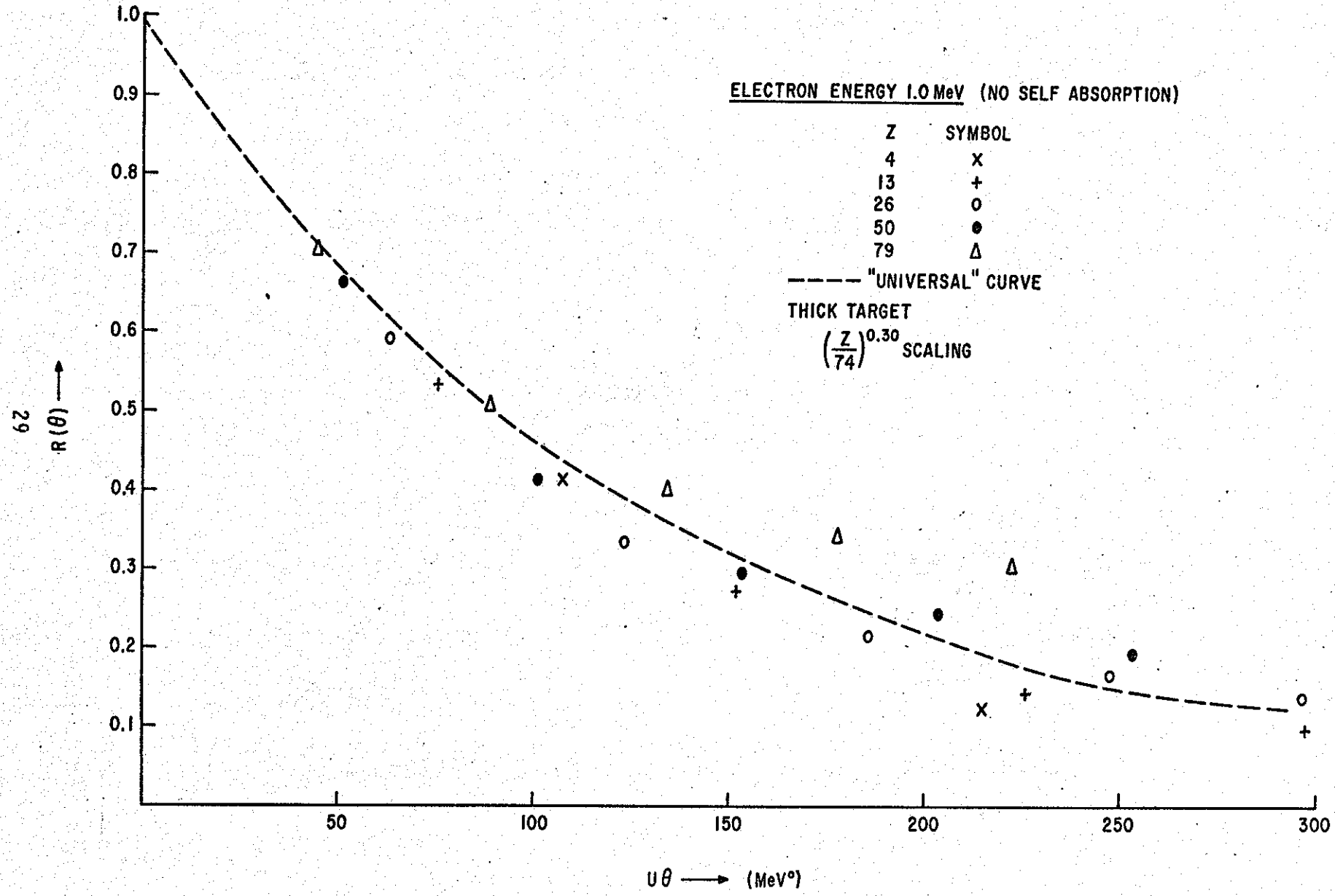
ELECTRON ENERGY 1.0 MeV (NO SELF ABSORPTION)
Z SYMBOL
4 X
13 +
26 o
50 ●
79 Δ
"UNIVERSAL" CURVE
THICK TARGET
$\left(\frac{Z}{74}\right)^{0.30}$ SCALING
$\frac{62}{29}$ R(θ) ⟶
1.0
0.9
0.8
0.7
0.6
0.5
0.4
0.3
0.2
0.1
50
100
150
200
250
300
Uθ ⟶ (MeV°)

FIGURE 3

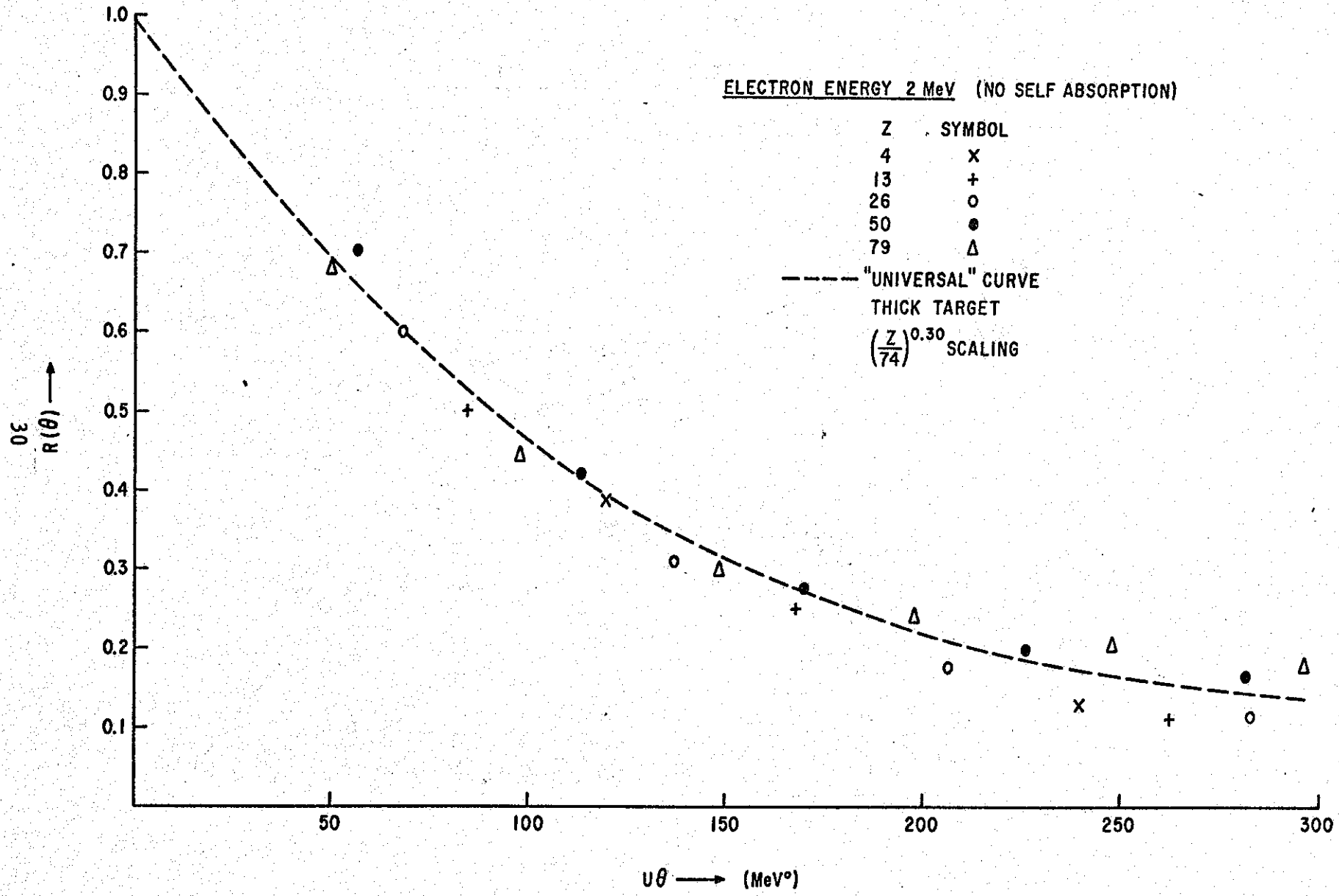
ELECTRON ENERGY 2 MeV (NO SELF ABSORPTION)
Z SYMBOL
4 X
13 +
26 o
50 ●
79 Δ
"UNIVERSAL" CURVE
THICK TARGET
$\left(\frac{Z}{74}\right)^{0.30}$ SCALING
$\frac{30}{R(\theta)}$ ⟶
1.0
0.9
0.8
0.7
0.6
0.5
0.4
0.3
0.2
0.1
50
100
150
200
250
300
Uθ ⟶ (MeV°)

FIGURE 4

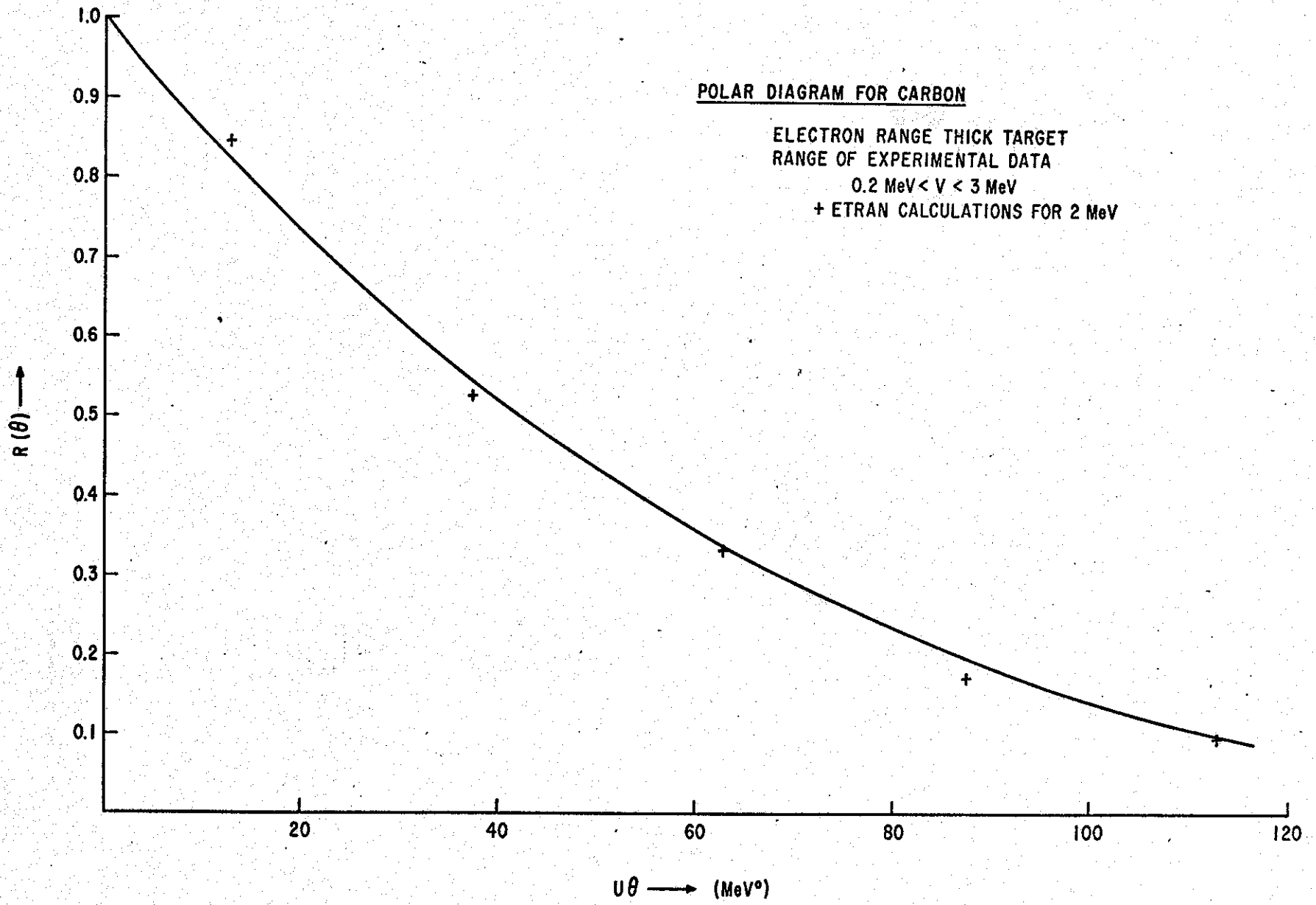
POLAR DIAGRAM FOR CARBON
ELECTRON RANGE THICK TARGET
RANGE OF EXPERIMENTAL DATA
0.2 MeV< V < 3 MeV
+ ETRAN CALCULATIONS FOR 2 MeV
R(θ) ⟶
1.0
0.9
0.8
0.7
0.6
0.5
0.4
0.3
0.2
0.1
20
40
60
80
100
120
Uθ ⟶ (MeV°)

FIGURE 5

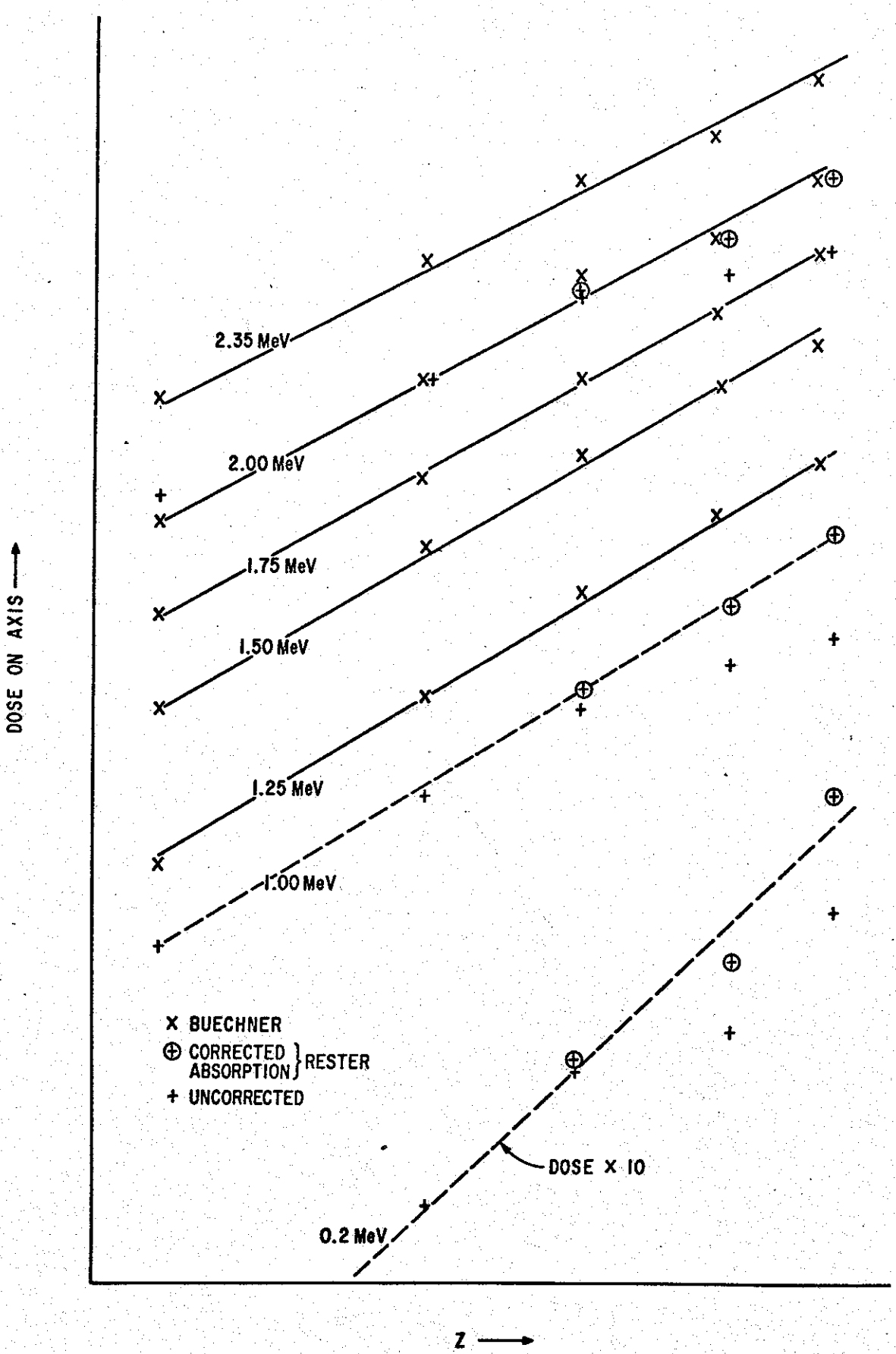
DOSE ON AXIS
2.35 MeV
2.00 MeV
1.75 MeV
1.50 MeV
1.25 MeV
1.00 MeV
0.2 MeV
X BUECHNER
⊕ CORRECTED ABSORPTION } RESTER
+ UNCORRECTED
DOSE X 10
Z

FIGURE 6

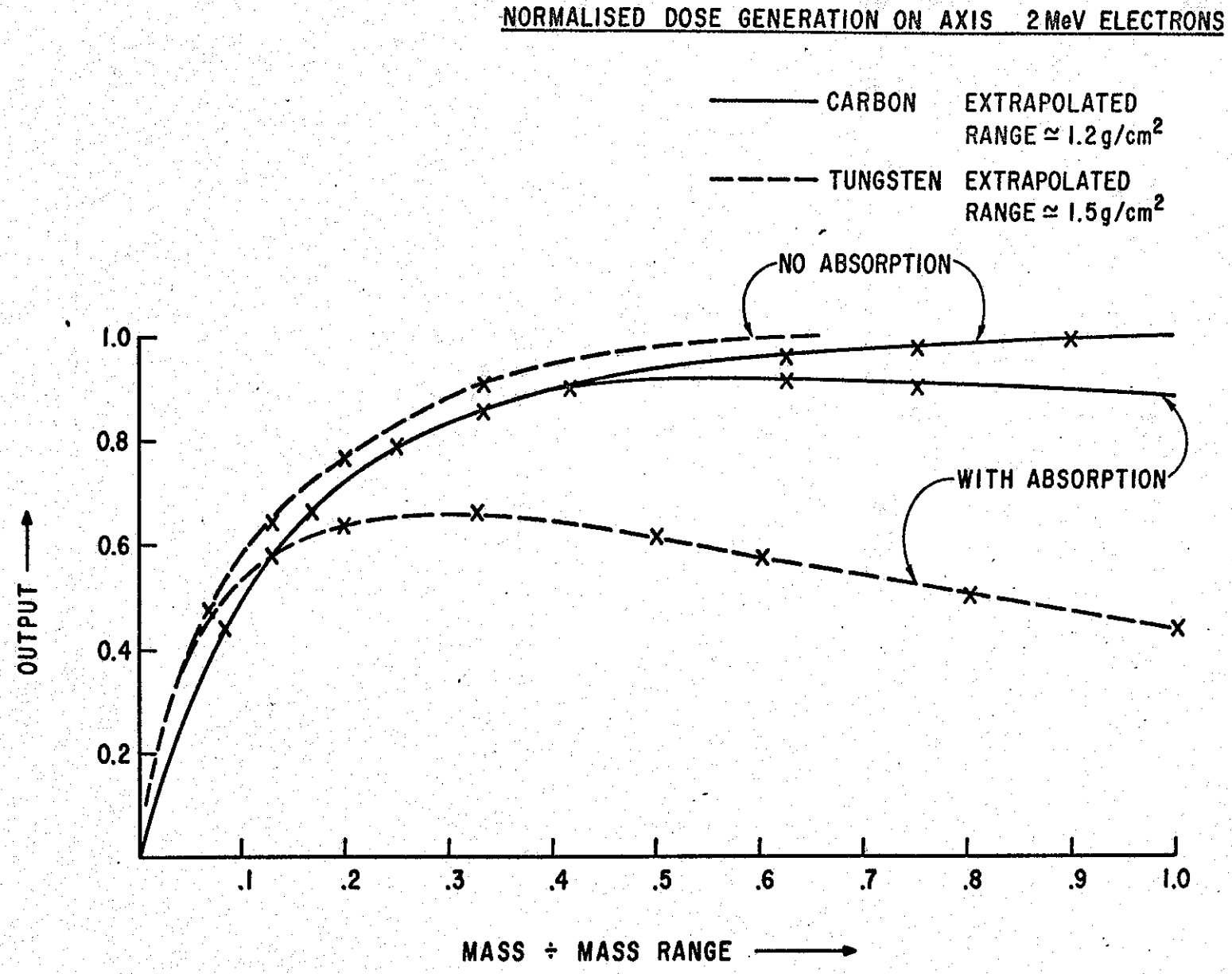
NORMALISED DOSE GENERATION ON AXIS 2 MeV ELECTRONS
CARBON EXTRAPOLATED RANGE ≃ 1.2 g/cm²
TUNGSTEN EXTRAPOLATED RANGE ≃ 1.5 g/cm²
NO ABSORPTION
WITH ABSORPTION
OUTPUT
1.0
0.8
0.6
0.4
0.2
.1
.2
.3
.4
.5
.6
.7
.8
.9
1.0
MASS ÷ MASS RANGE

FIGURE 7

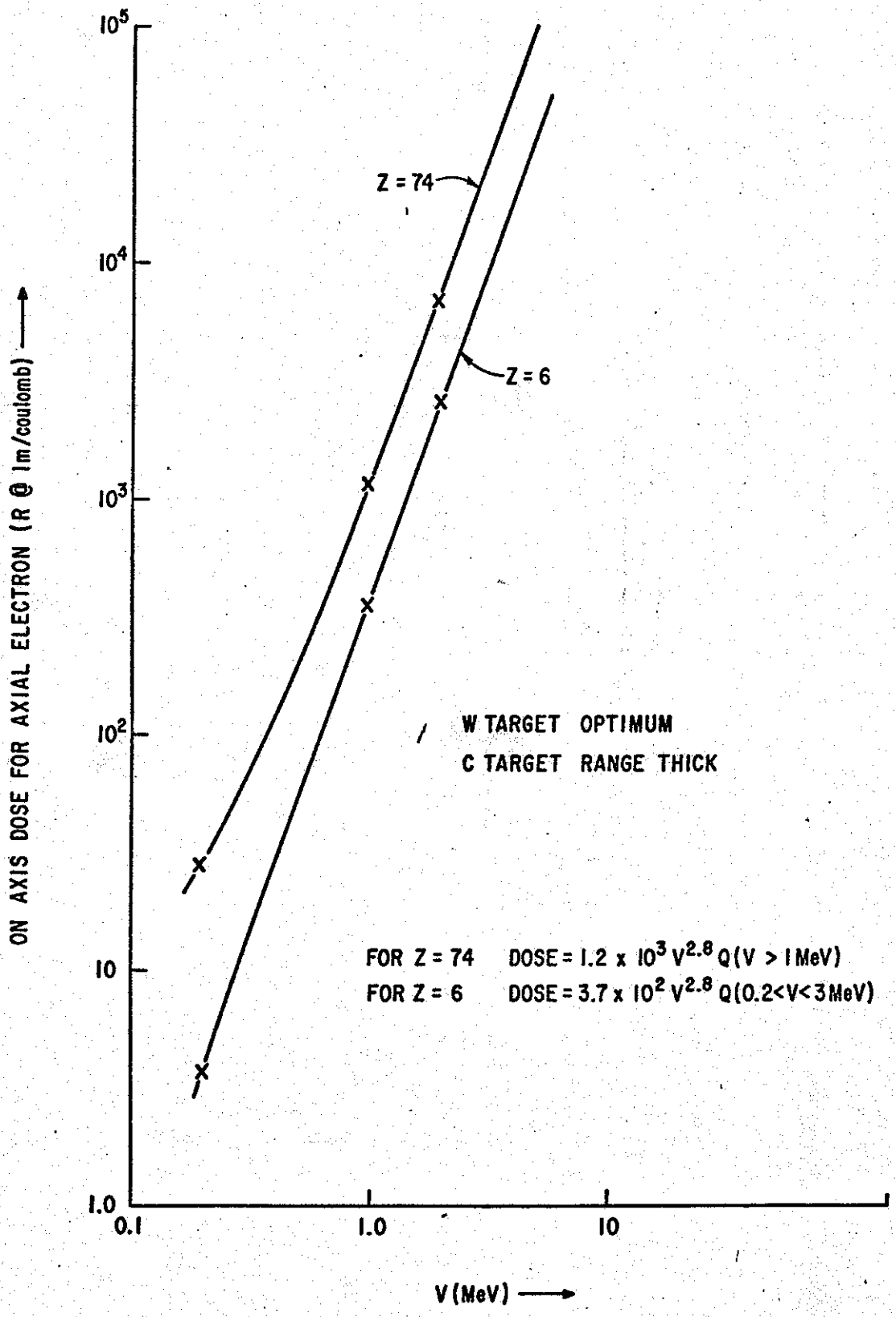
ON AXIS DOSE FOR AXIAL ELECTRON (R @ 1m/coulomb)
10^5
10^4
10^3
10^2
10
1.0
0.1
1.0
10
V (MeV)
Z = 74
Z = 6
W TARGET OPTIMUM
C TARGET RANGE THICK
FOR Z = 74 DOSE = 1.2 x 10^3 $V^{2.8}$ Q(V > 1 MeV)
FOR Z = 6 DOSE = 3.7 x 10^2 $V^{2.8}$ Q(0.2<V<3 MeV)

FIGURE 8

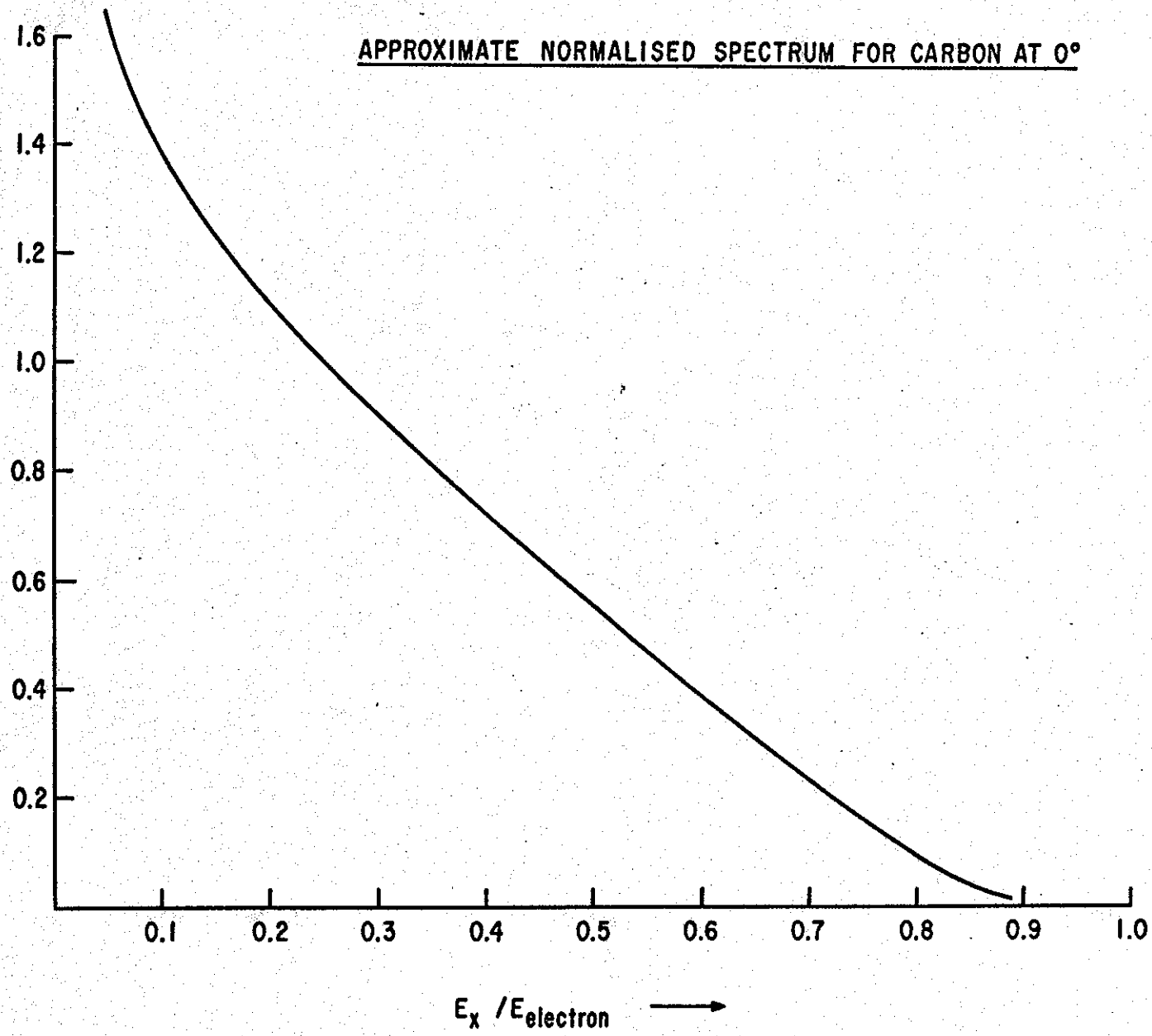
APPROXIMATE NORMALISED SPECTRUM FOR CARBON AT 0°
1.6
1.4
1.2
1.0
0.8
0.6
0.4
0.2
0.1
0.2
0.3
0.4
0.5
0.6
0.7
0.8
0.9
1.0
E_x /$E_{electron}$

FIGURE 9

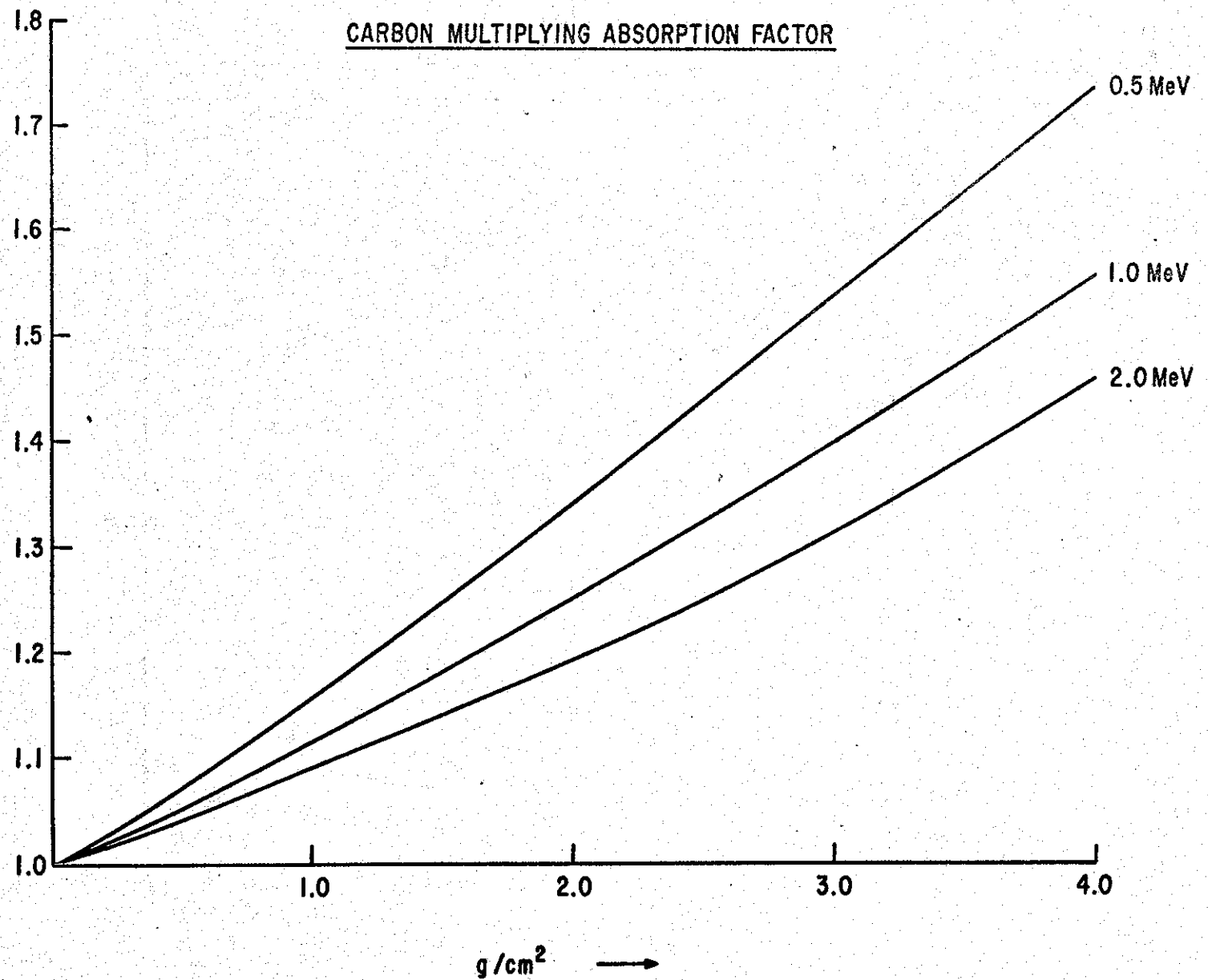
CARBON MULTIPLYING ABSORPTION FACTOR
1.8
1.7
1.6
1.5
1.4
1.3
1.2
1.1
1.0
0.5 MeV
1.0 MeV
2.0 MeV
1.0
2.0
3.0
4.0
g/cm²

FIGURE 10

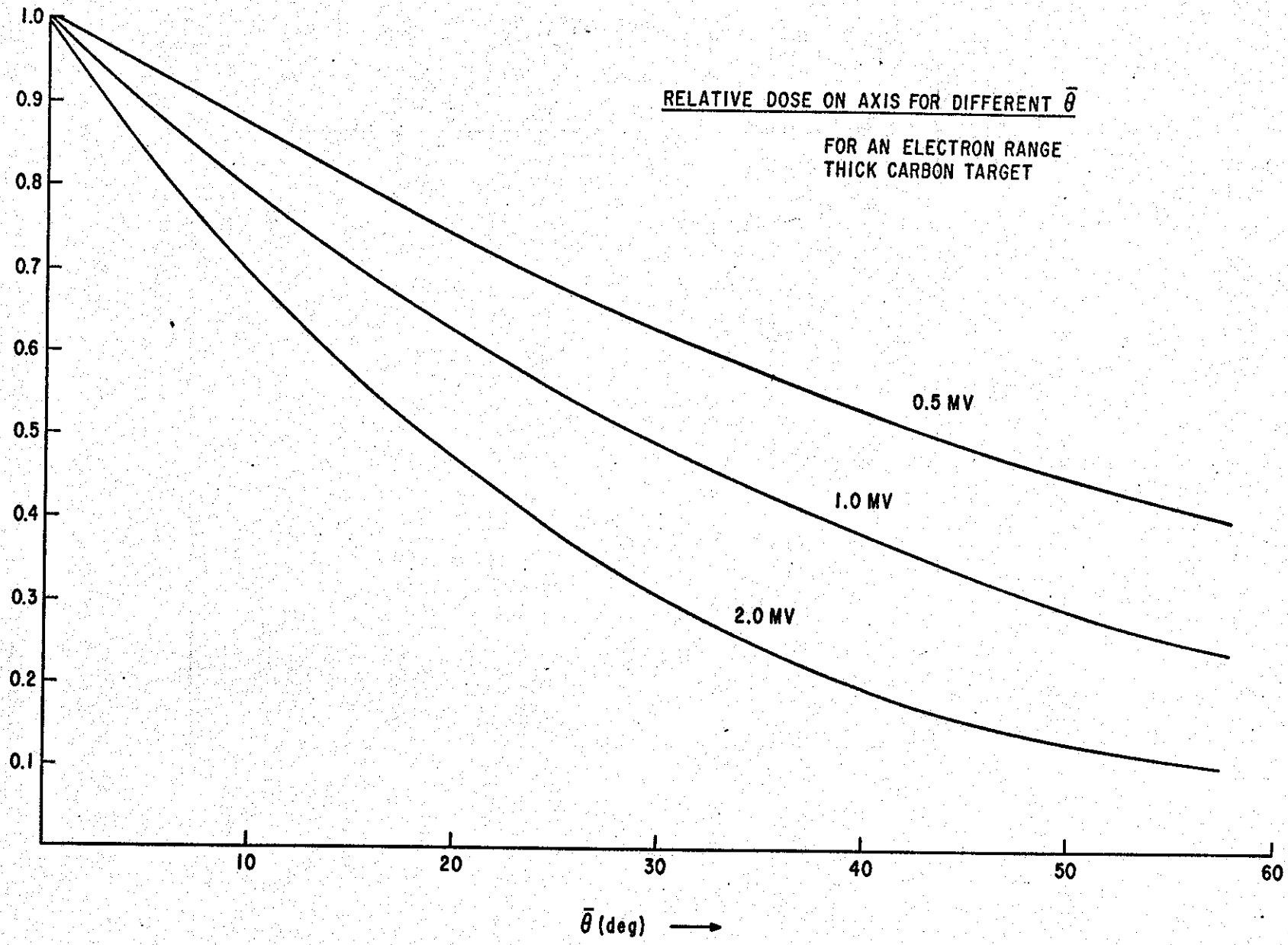
RELATIVE DOSE ON AXIS FOR DIFFERENT $\bar{\theta}$
FOR AN ELECTRON RANGE THICK CARBON TARGET
0.5 MV
1.0 MV
2.0 MV
1.0
0.9
0.8
0.7
0.6
0.5
0.4
0.3
0.2
0.1
10
20
30
40
50
60
$\bar{\theta}$ (deg) ⟶

FIGURE 11

TLD. COPPER SHIELDED MULTIPLYING ABSORPTION FACTOR

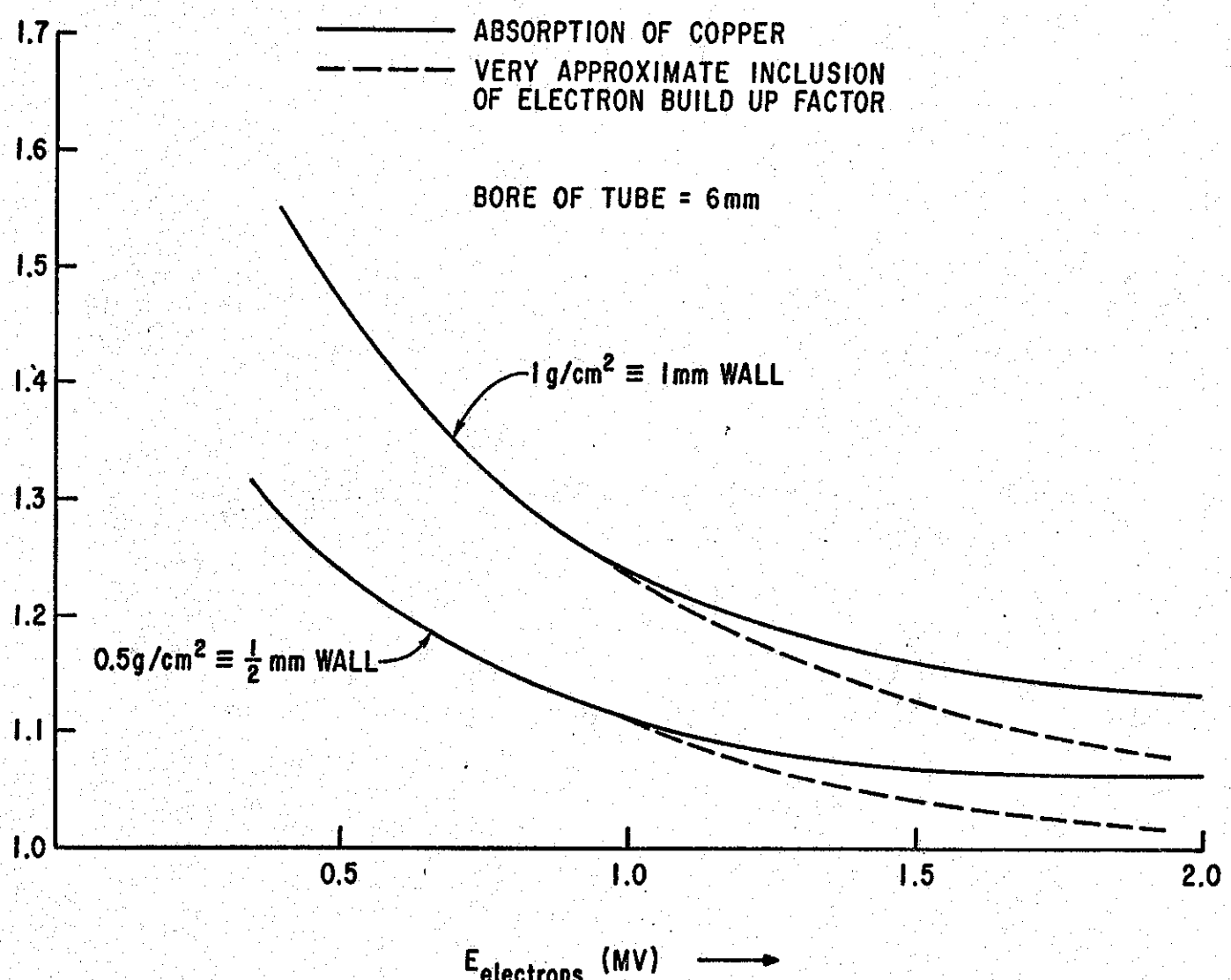

FIGURE 12

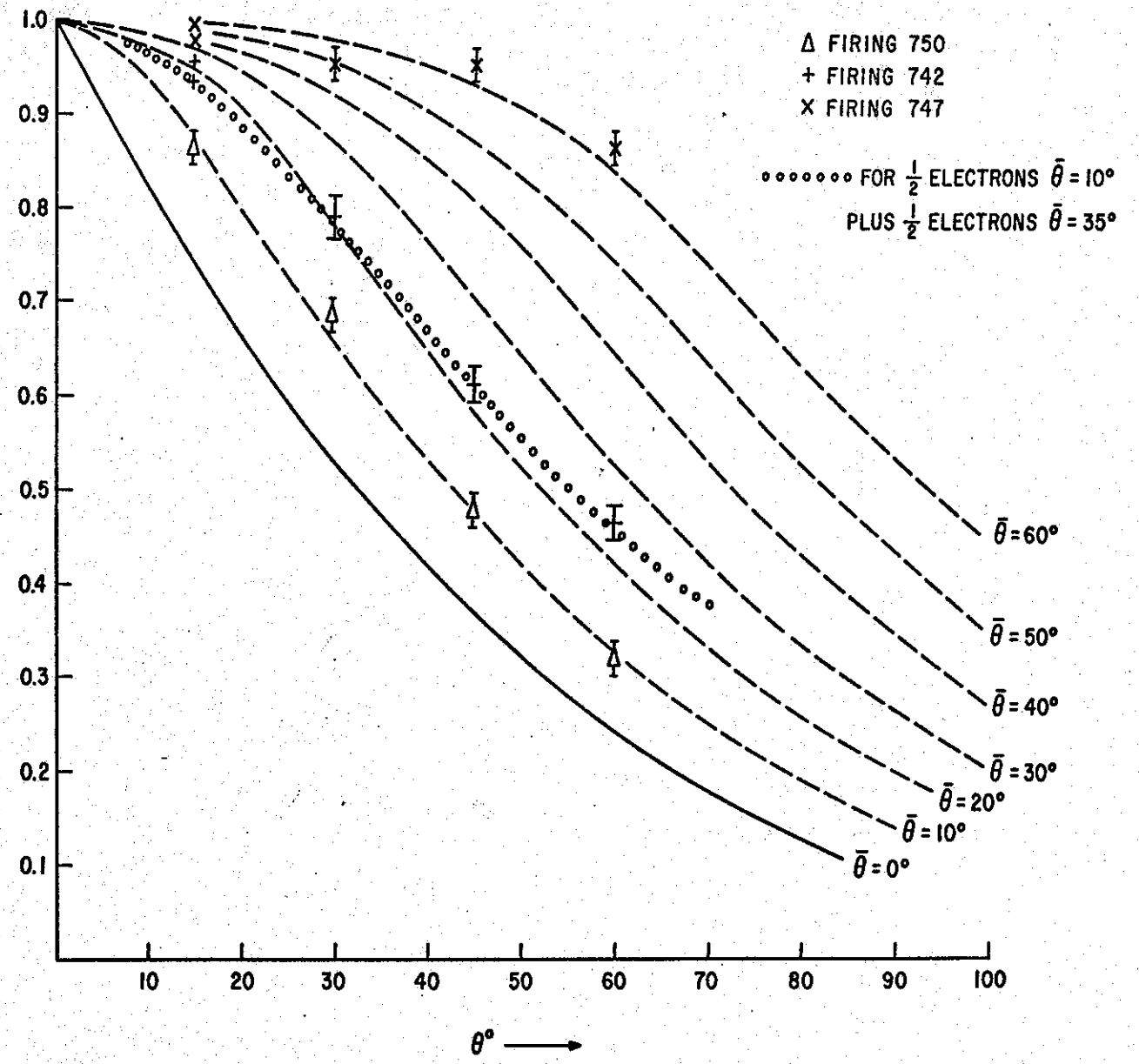
Δ FIRING 750
+ FIRING 742
X FIRING 747
FOR ½ ELECTRONS θ̄ = 10°
PLUS ½ ELECTRONS θ̄ = 35°
θ̄ = 60°
θ̄ = 50°
θ̄ = 40°
θ̄ = 30°
θ̄ = 20°
θ̄ = 10°
θ̄ = 0°
R(θ)
θ°
1.0
0.9
0.8
0.7
0.6
0.5
0.4
0.3
0.2
0.1
10
20
30
40
50
60
70
80
90
100

FIGURE 13

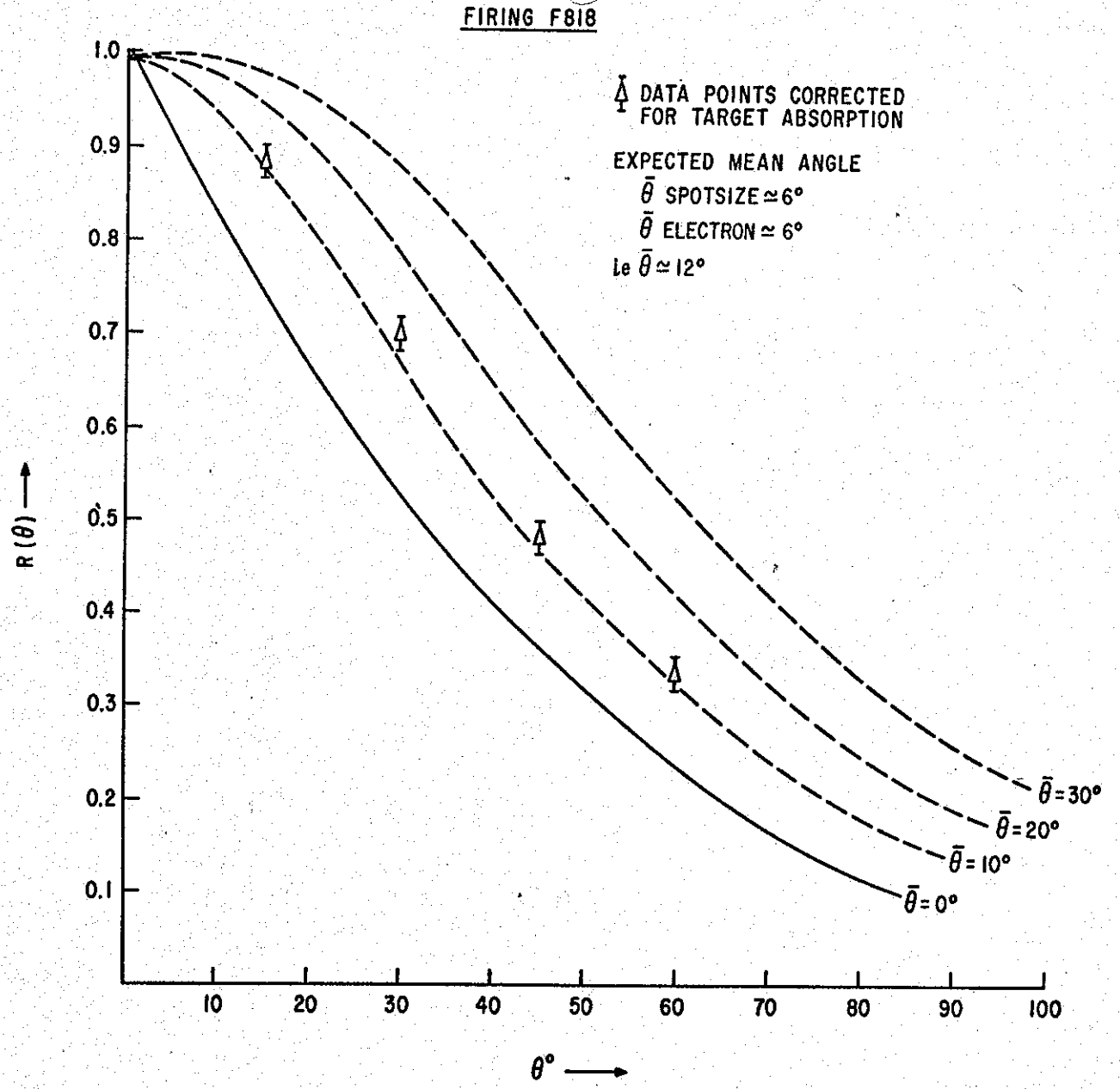
FIRING F818
DATA POINTS CORRECTED FOR TARGET ABSORPTION
EXPECTED MEAN ANGLE
$\bar{\theta}$ SPOTSIZE ≃ 6°
$\bar{\theta}$ ELECTRON ≃ 6°
Le $\bar{\theta}$ ≃ 12°
$\bar{\theta}$=30°
$\bar{\theta}$=20°
$\bar{\theta}$=10°
$\bar{\theta}$=0°
R(θ) ⟶
θ° ⟶
1.0
0.9
0.8
0.7
0.6
0.5
0.4
0.3
0.2
0.1
10
20
30
40
50
60
70
80
90
100

FIGURE 14

FIRING 818 ONE RAZOR BLADE A-K GAP 1.5 cm

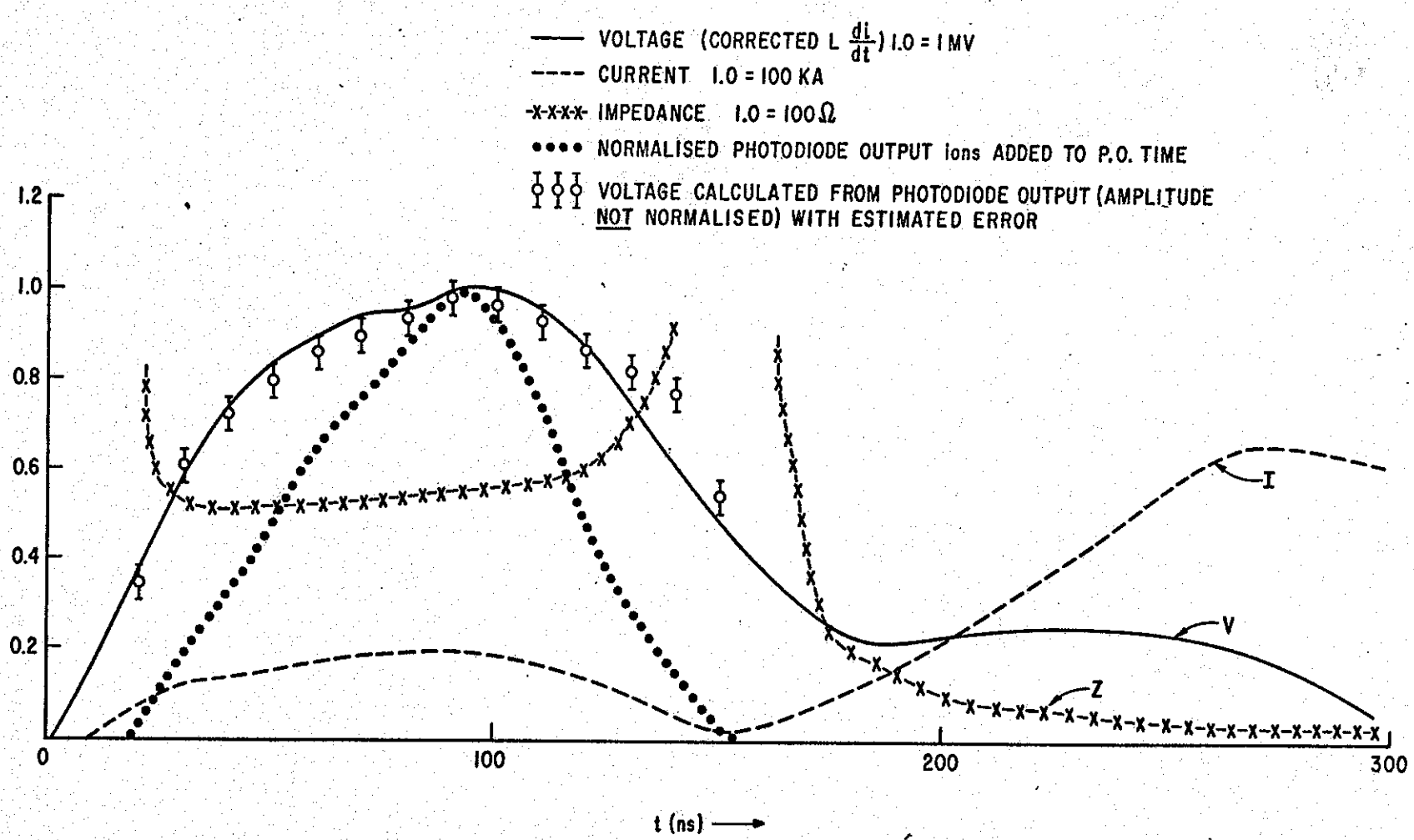

FIGURE 15

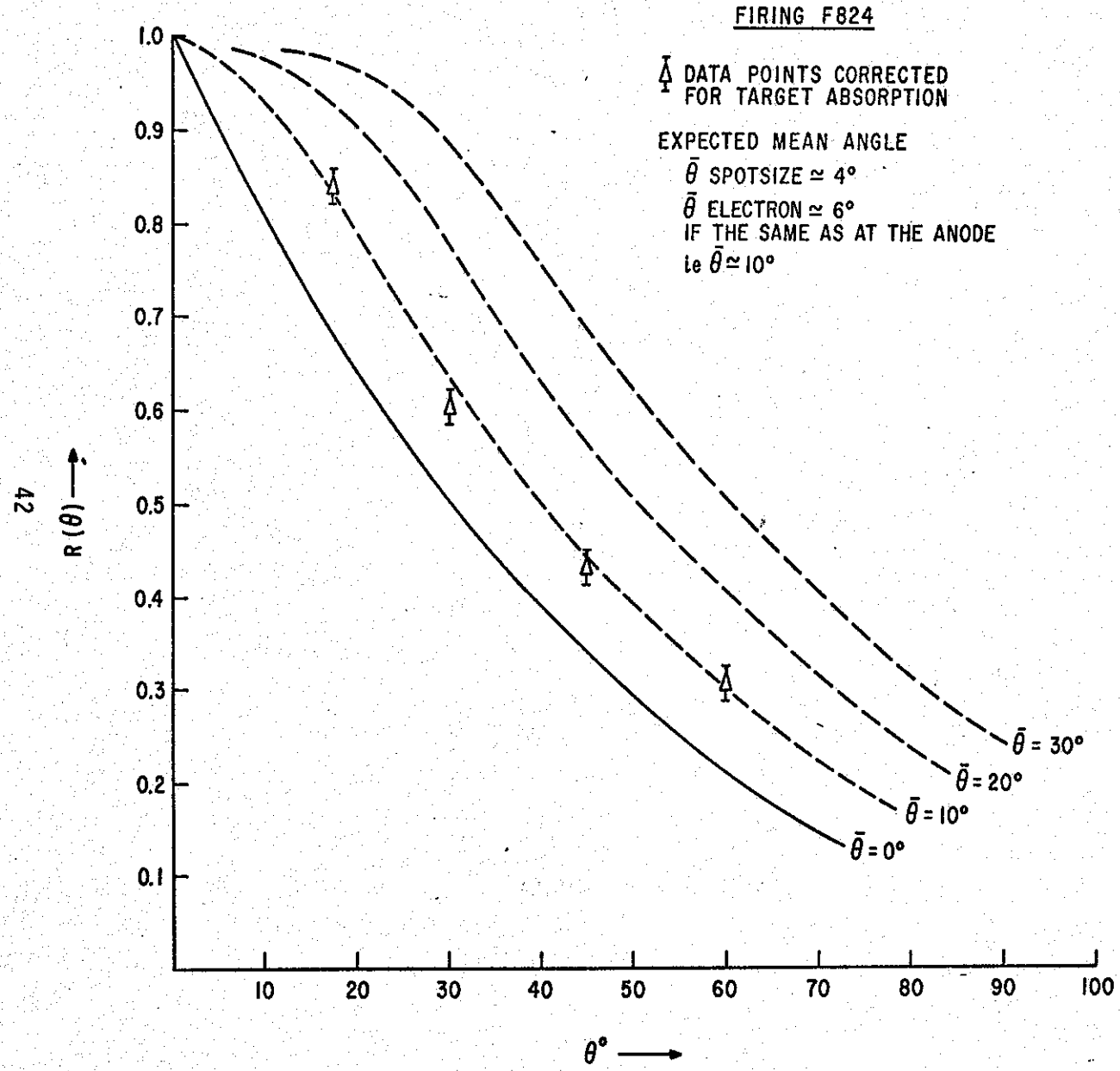
FIRING F824
DATA POINTS CORRECTED FOR TARGET ABSORPTION
EXPECTED MEAN ANGLE
$\bar{\theta}$ SPOTSIZE ≃ 4°
$\bar{\theta}$ ELECTRON ≃ 6°
IF THE SAME AS AT THE ANODE
ie $\bar{\theta}$ ≃ 10°
$\bar{\theta}$ = 30°
$\bar{\theta}$ = 20°
$\bar{\theta}$ = 10°
$\bar{\theta}$ = 0°
R(θ) →
θ° →
1.0
0.9
0.8
0.7
0.6
0.5
0.4
0.3
0.2
0.1
10
20
30
40
50
60
70
80
90
100

FIGURE 16

FIRING 824 ONE RAZOR BLADE WITH 34 Ω's DRIFT

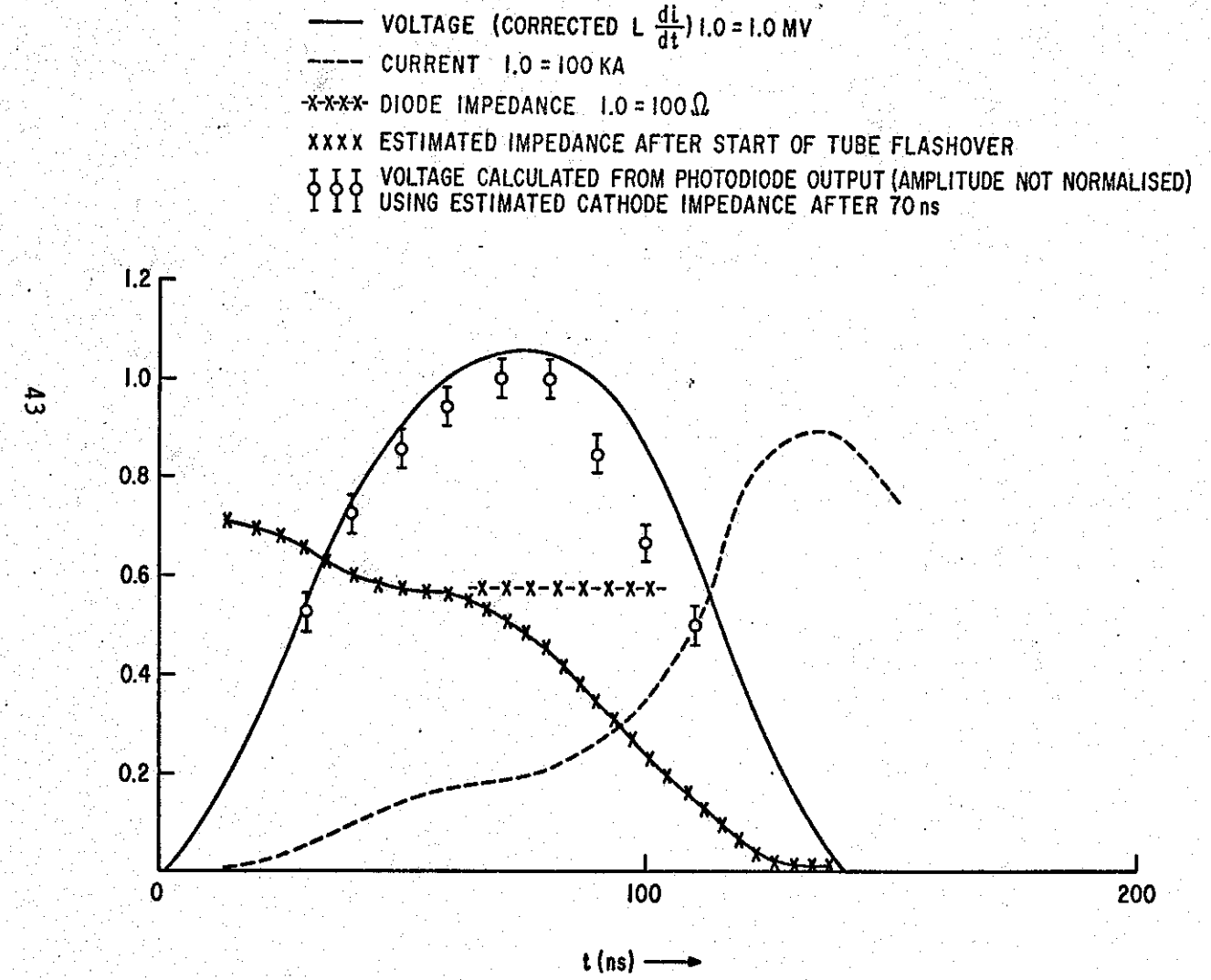

FIGURE 17

FIRING 819 SIX RAZOR BLADES PLUS LOW PRESSURE DRIFT

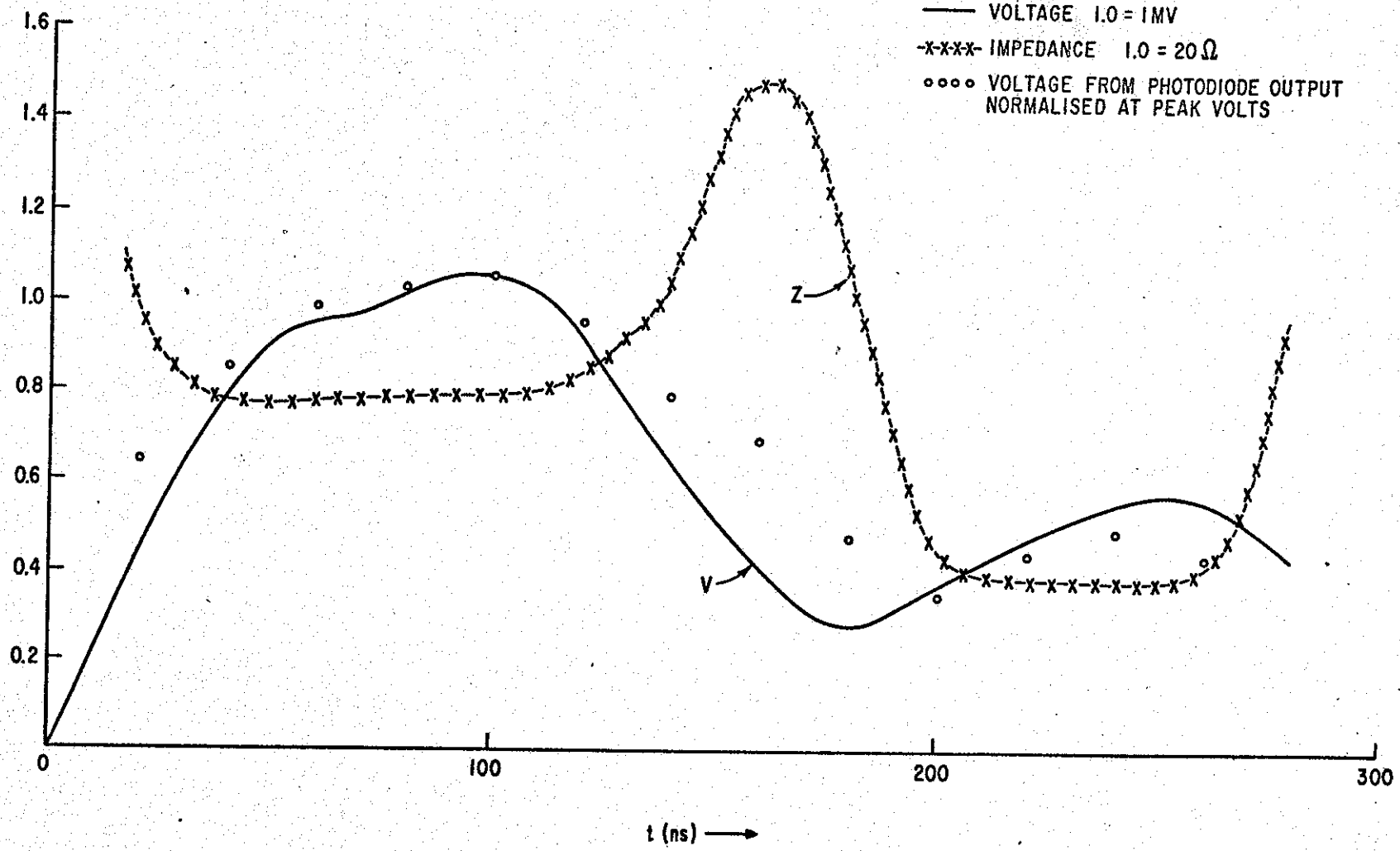

FIGURE 18